Roehrich, A. D., Bordignon, E., Mode, S., Da-kang, S., Liu, X., Pain, M., Murillo, I., Martinez-Argudo, I., Sessions, R. B., & Blocker, A. J. (2017). Steps for Shigella Gatekeeper MxiC Function in Hierarchical Type III Secretion Regulation. *Journal of Biological Chemistry*, *292*(5), 1705-1723. https://doi.org/10.1074/jbc.M116.746826

Steps for *Shigella* Gatekeeper MxiC Function in Hierarchical Type III Secretion Regulation

A. Dorothea Roehrich[1,a], Enrica Bordignon[2,b], Selma Mode[1], Da-Kang Shen[1], Xia Liu[1], Maria Pain[1], Isabel Murillo[1], Isabel Martinez-Argudo[1,3], Richard B. Sessions[4] and Ariel J. Blocker[1*]

[1]Schools of Cellular & Molecular Medicine and Biochemistry, Medical Sciences Building, Faculty of Medical and Veterinary Sciences, University of Bristol, BS8 1TD, United Kingdom; [2] Fachbereich Physik, Freie Universität Berlin, 14195 Berlin, Germany; [3]Área de Genética, Facultad de Ciencias Ambientales y Bioquímica, Universitdad de Castilla-La Mancha, E-45071, Toledo, Spain; [4] School of Biochemistry, Medical Sciences Building, Faculty of Medical and Veterinary Sciences, University of Bristol, BS8 1TD, United Kingdom

Running title: Genetic & biophysical study of *Shigella* T3SS component MxiC

To whom correspondence should be addressed: Ariel Blocker, School of Cellular and Molecular Medicine, University of Bristol, University Walk, Bristol, BS8 1TD, UK; Telephone: +44 (0) 117 3312063; Email: ariel.blocker@bristol.ac.uk

Keywords: gram-negative bacteria; protein secretion; cellular regulation; molecular genetics; biophysics; MxiC; *Shigella*, type III secretion system; electron paramagnetic resonance

ABSTRACT

Type III secretion systems are complex nanomachines used for injection of proteins from Gram-negative bacteria into eukaryotic cells. While they are assembled when the environmental conditions are appropriate, they only start secreting upon contact with a host cell. Secretion is hierarchical: first, the pore-forming translocators are released, next, effector proteins are injected. Hierarchy between these protein classes is mediated by a conserved gate-keeper protein, MxiC in *Shigella*. As its molecular mechanism of action is still poorly understood, we used its structure to guide site-directed mutagenesis and dissect its function. We identified mutants predominantly affecting all known features of MxiC regulation: secretion of translocators, MxiC and/or effectors. Using molecular genetics we then mapped at which point in the regulatory cascade the mutants were affected. Analysis of some of these mutants led us to a set of electron paramagnetic resonance experiments that provide evidence that MxiC interacts directly with IpaD. We suggest how this interaction regulates a switch in its conformation that is key to its functions.

INTRODUCTION

Type III secretion systems (T3SSs) are central devices in the virulence of many major Gram-negative bacterial pathogens of humans, animals and plants. They translocate virulence proteins into the membranes and cytoplasm of eukaryotic host cells to manipulate them during infection. T3SSs are key to the virulence of enteric pathogens such as *E. coli*, *Salmonella* and *Shigella* species.

Shigella species are the etiological agent of bacillary dysentery in humans. The *Shigella* T3SS consists of a cytoplasmic portion and a transmembrane region traversing both bacterial membranes, into which a hollow needle, made of MxiH, is embedded protruding from the bacterial surface (2). Physical contact with eukaryotic host cells activates the secretion system, which initiates secretion and leads to creation of a pore, formed by the bacterial proteins IpaB and IpaC, in host-cell membranes (3). The effectors are translocated through the needle (4) and pore channels, to facilitate host cell invasion (3). The needle tip complex (TC), which contains IpaD and IpaB, is the host cell sensor and transforms itself into the translocation pore (5) via addition of IpaC upon secretion activation (6,7). IpaD is hydrophilic and required for tip recruitment of the other two proteins, which are hydrophobic, and hence chaperoned by IpgC intrabacterially (8). The three proteins are collectively called the translocators.

T3SSs are assembled, using a broadly conserved morphogenesis pathway (9), following

detection of environmental cues indicating entry into the host. In addition, virulence effectors acting late in the host cell manipulation cascade are only expressed once the presynthesised early effectors have been secreted at host cell contact. Most components and/or molecular mechanisms of these regulatory pathways diverge from one T3SS-carrying organism to another (10). Yet, one regulatory cascade is conserved, a process allowing hierarchical secretion of substrates, although the stages it covers vary: needle vs. translocator components in plant pathogens or translocators and then early effectors in animal ones (11).

We focus here on how this cascade functions in animal pathogens. After T3SS assembly, effector secretion is prevented through the concerted action of surface TC proteins and regulators that control secretion from within the bacterial cytoplasm. The TC may prevent premature effector secretion by allosterically constraining the T3SS in a secretion "off" conformation without blocking the secretion channel (12-14). Upon physical contact of the TC with host cells, a signal, termed Signal 1, is transmitted via the TC (15) and needle (12,16) to the cytoplasm where it triggers secretion. Next, translocators are secreted to form the pore in the host cell membrane (3). Successful pore formation at the needle tip generates Signal 2, also transmitted via the needle, that allows inactivation or T3S-mediated removal of a conserved cytoplasmic regulatory protein, MxiC in *Shigella* (12,16). Third, early effector proteins are secreted and translocated into the host cell and late effector expression is activated (17).

MxiC belongs to a class of "gate-keeper" proteins that is conserved among different type III secretion systems (18). They repress effector secretion in the absence of a secretion signal, but have different roles in translocator secretion, impairing it in a Δ*mxiC* mutant (12) while stimulating it in a *Yersinia ΔyopN* mutant (19). While gate-keepers are clearly involved in the cytoplasmic steps controlling T3SS secretion hierarchy upon activation, their mechanism of action remains unclear.

The gate-keepers have conserved structures (20,21): after an N-terminal secretion signal and putative chaperone-binding domain (CBD), three α-helical X-bundles (domains 1-3; supplemental Fig. S1A-C) form a flat, elongated structure (21) typical for "hub proteins" regulating processes via interaction with multiple partners. In some species, gate-keepers are composed of two proteins where the second polypeptide covers the C-terminal X-bundle (domain 3; supplemental Fig. S1D-E (20)).

MxiC is secreted by the type III secretion system (22). Its N-terminal 30 residues contain the secretion signal (23). Immediately thereafter is a domain similar to the chaperone-binding domain of *Yersinia* YopN (20,21). This domain is partially conserved (18) even though not every MxiC homologue has an identified chaperone. While this area is enriched in hydrophobic residues that mediate interactions with the chaperones, fewer hydrophobic residues are found in MxiC.

Many type III secreted proteins are bound by a chaperone inside the bacterium. These chaperones have various roles, including stabilisation of their binding partners, aiding their secretion and mediation of secretion hierarchy (24). Several MxiC homologues bind to specific heterodimeric chaperones. For instance, *Yersinia* YopN binds to the SycN/YscB heterodimer (20,25). It wraps around its heterodimeric chaperone in a conformation similar to other effector/chaperone complexes (20). This domain is disordered in the absence of the chaperones. Interestingly, the first ~75 residues of MxiC are likely also disordered (21). Yet, so far no chaperone has been identified for MxiC (23).

MxiC's helix 9 of is a straight helix, while the structurally equivalent helix in YopN/TyeA is kinked into two smaller helices. The structure of the EPEC MxiC homolog, SepL, is also bent at an equivalent location (26). Thus, one face of the molecule is flat in MxiC, while it is concave in YopN/TyeA and SepL (21,26). Interestingly, this surface contains a negatively charged patch (E201, E276, E293; (21)) we showed is important for MxiC functions that involve IpaD (15). Furthermore, the *Chlamydia* hydrophobic translocator chaperone Scc3 binds to its gate-keeper at the flat interface between domain 2 and 3 (27), which the kink in the YopN/TyeA renders convex. Deane et al. (2008) already suggested this

structural difference between MxiC and YopN/TyeA could be a "conformational switch" and these new findings suggest it might allow the switch from hydrophilic to hydrophobic translocator secretion.

To dissect MxiC's interconnected functions we used site-directed mutagenesis. Mutant design was guided by the description of MxiC structure by Deane et al. (2008) and the sequence alignment of MxiC homologues by Pallen et al. (2005) (18). Our mutations (Fig. 1) focussed on the N-terminal non-crystallised region and domains 2 and 3 of the crystal structure (21). We identified mutants predominantly affecting all known features of MxiC regulation: secretion of translocators, MxiC and effectors. Using molecular genetics to map at which point in the regulatory cascade the mutants were affected we further dissected MxiC's role. Analysis of some of these mutants led us to electron paramagnetic resonance (EPR) experiments that, together with phenotypic analysis of the mutants, provide evidence that MxiC's conformation is regulated via a direct interaction with IpaD.

RESULTS

MxiC's secretion signal is not required for promoting inducible translocator secretion

A non-secretable form of MxiC lacking residues 2 to 30 is unable to prevent effector secretion (23). However, MxiC also regulates inducible translocator secretion (12). This had not yet been characterised when the *mxiCΔNterm* mutant was first described. We thus investigated whether MxiC's two roles could be uncoupled.

We generated a *mxiCΔNterm* mutant equivalent to that of Botteaux et al. (2009). In our hands, MxiCΔNterm was unstable: while wild-type *mxiC* was induced to wild-type levels after addition of 25 µM IPTG, *mxiCΔNterm* was only expressed at similar levels after addition of 100 µM IPTG. Furthermore, MxiCΔNterm seemed partially degraded (Fig. 2B).

As previously described, MxiCΔNterm is not secreted after Congo red (CR) induction (Fig. 2A and (23)) and effector proteins are leaked ((23) and data not shown). Furthermore, MxiCΔNterm was not secreted in a *ΔipaB* constitutive secreter background (supplemental Fig. S2), indicating deletion of the N-terminus affects its ability to become secreted. However, secretion of IpaB, IpaC and IpaD was unaffected in *mxiCΔNterm*: small differences between *ΔmxiC*/*mxiC*+ and *mxiCΔNterm* were not statistically significant (Fig. 2A and C). Thus, MxiC's ability to prevent effector secretion and to promote inducible translocator secretion are not coupled and only the former requires its secretion signal.

MxiC's C-terminus is essential

The 11 C-terminal residues of the EPEC MxiC homolog, SepL, are required for regulation of effector secretion but not for translocator secretion (28). As a complementary experiment, we deleted the last 14 residues of MxiC (Fig. 1B), which are equivalent to the last eleven residues of SepL ((18) and supplemental Fig. S3). The resulting *mxiCΔCterm* mutant was stably expressed, but unable to complement *ΔmxiC* (supplemental Fig. S4): translocators were only weakly induced and effector proteins were leaked. In addition, MxiCΔCterm itself was only poorly secreted (supplemental Fig. S4), even in *ΔipaB* (supplemental Fig. S2). Therefore, unlike for SepL, MxiC's C-terminus is essential.

The putative chaperone-binding domain of MxiC regulates its secretion, and hence that of effectors

The chaperone-binding domain of YopN has a chaperone-independent role in secretion regulation (29). We thus wondered whether MxiC's putative chaperone-binding domain is required for its function. First, we deleted the whole CBD (Fig. 1A) to generate *mxiCΔCBD*, lacking residues 32-72). This construct was stably expressed, but leaked and only weakly secreted upon CR induction (Fig. 3A). Interestingly, secretion of MxiCΔCBD was enhanced in a *ΔipaB* background (supplemental Fig. S2). This indicates the chaperone-binding domain influences the regulation of MxiC secretion rather than the intrinsic ability of the protein to become secreted. Furthermore, while *mxiCΔCBD* could not block effector secretion, it was able to promote translocator secretion (Fig. 3A).

Next, we investigated which YopN residues contacting the chaperones are conserved in MxiC. As the alignment of this area is ambiguous (supplemental Fig. S5), we made several single and combined charge-swap mutations. *mxiCK66E* was unable to complement *ΔmxiC*. Paradoxically, the mutant protein was detected in culture supernatants and, to a lesser degree, in the supernatants after CR induction, but only low levels were detected in whole culture lysates (Fig. 3C). *mxiC(D46K,D49K)* had a wild-type like phenotype, except for some premature MxiC secretion. *mxiC(D46K,D49K,K66E)* leaked MxiC at high levels and was unable to prevent effector secretion (data not shown). A similar phenotype was observed in *mxiCK68E* (Fig. 3). Furthermore, *mxiCK68E* and *mxiCK66E,* but not *mxiCΔCBD,* displayed reduced induction of translocator secretion, suggesting the effect of the point mutations on translocator secretion is indirect. Therefore, the putative chaperone-binding domain is required for regulating MxiC secretion and for preventing effector secretion.

MxiC lacking its secretion signal is not secreted and also unable to prevent effector secretion (23). In a *mxiHK69A* mutant where MxiC is not secreted, effectors are also not released (12,16). Thus, there is a correlation between "secretability" and ability to block secretion. We hence tested whether MxiC needs to be quantitatively removed from the cytoplasm to release the block on effector secretion. We compared the levels of several secreted proteins in supernatants after induction with CR with levels in the corresponding total cultures, i.e. samples containing secreted and intracellular proteins. The translocators IpaB and IpaC were secreted nearly completely, while only 8±6% of MxiC was secreted in the same period (supplemental Fig. S6). Translocator IpaD and early effector IpgD were secreted at intermediate levels of ca. 40% to 50%. Thus, either only a small proportion of intracellular MxiC is involved in blocking secretion, and/or its secretion *per se* is not required to release this block.

Any MxiC chaperone remains unidentified

As MxiC's putative CBD is essential for regulating the protein's secretion and as *Yersinia* YopN needs its heterodimeric chaperone SycN/YscB for efficient secretion and regulation (25,30), we wondered whether a chaperone is required for MxiC function. Three chaperones are encoded on the pWR100 virulence plasmid of *Shigella* that fall into the same general class as SycN and YscB: IpgA, IpgE and Spa15 (31). Botteaux et al. (2009) already found lack of any of these proteins alone has no effect on MxiC secretion or stability. Thus, none of *Shigella* Class I chaperones in works like SycN/YscB. However, their mechanism of action could be different and thus we generated two double deletions (*ΔipgEΔspa15* and *ΔipgEΔipgA*) and a triple deletion (*ΔipgEΔipgAΔspa15*). However, even the deletion of multiple chaperones had no effect on MxiC (supplemental Fig. S7). This suggests that none of these chaperones influences MxiC function. Therefore, either there are no such chaperones binding to the CBD of MxiC or we have not identified them because of low sequence similarities. However, we think the latter is unlikely because MxiC is primarily monomeric in cytosol and no known Class 1 chaperone was identified, even using mass spectrometry after crosslinking (32).

A hydrophobic patch on the surface of MxiC is required for blocking effector secretion

Deane et al. (2008) noticed conservation of a patch of hydrophobic residues on the surface of MxiC's domain 2 (Fig. 1B; L222, M226, G239, L242 and L245), suggesting it as a site for protein-protein interactions. Cherradi et al. (2013) change single residues in this patch to alanines (33). MxiC is not detectable in *mxiCL222A* and *mxiCL242A*, while three other mutations (M226A, G239A and L245A) do not effect its function. We mutated residues L222 and L242 into serines and found that neither *mxiCL222S* and *mxiCL242S*, nor the double mutant *mxiC(L222S, L242S)* had any effect on MxiC stability or function (data not shown).

As change to a polar side chain may not have been enough to disrupt interactions in this area, we introduced two charges. The *mxiC(M226K, L242D)* mutant was stably expressed (Fig. 4C) and able to induce translocator secretion after induction (Fig. 4A). However, *mxiC(M226K,L242D)* was unable to prevent effector secretion (Fig. 4A-B). Thus, the hydrophobic patch is involved in preventing effector secretion.

Mutations in a putative "hinge" area of MxiC lead to altered secretion patterns

The sequence in MxiC helix 9, its putative "hinge" region (Fig. 1A), is not conserved. But, it contains multiple serines, aspartates, valines and threonines that are not classically helix favouring (34). Multiple secondary structure prediction programmes suggest that even in MxiC, helix 9 would be broken (supplemental Fig. S8B). We generated a model of the "bent" wild-type protein using the YopN/TyeA structure (PDB code 1XL3, (20)) as template (supplemental Fig. S8A). In comparison to the crystal structure, the "bent" MxiC model is not only folded at the hinge region, but undergoes a slight twisting motion. We then made three mutants: one mutant introducing a proline (V256P; "bent") that would likely cause a break in helix 9 and thus a conformation similar to that of YopN/TyeA, a second mutant introducing three glycines (T253G, S254G, D255G; "wobble") in the area to favour switching between both putative forms and a third mutant that might stabilise a straight helix (I251A, T253A, S254A, D255E; "straight"). MxiC I251 is structurally equivalent to F268 of YopN, which is sandwiched between hydrophobic residues in the core of TyeA, thus likely stabilising the bent conformation.

All mutant proteins were expressed at wild-type levels or better (Fig. 5C). The triple-glycine mutant *mxiC(T253G,S254G,D255G)* behaved like *ΔmxiC*. MxiC was not secreted efficiently, translocator secretion was reduced (43 ± 23% of the complemented strain) and effector proteins were leaked. In the "straight" mutant *mxiC(I251A,T253A,S254A,D255E)*, induced secretion of both IpaB and IpaC was reduced, while that of IpaD was as efficient as in the complemented strain, or even increased (Fig. 5D). This mutant did not affect secretion of MxiC or effector proteins. The "bent" mutant *mxiCV256P* leaked high levels of a low molecular weight protein. We identified this band by mass spectrometry using a sample equivalent to the "-CR" sample in Fig. 5A. The top T3S-related protein identified was effector IpgB1 (6% of the total protein content). The similarly-sized effector/anti-activator OspD1 was not detected in this band. The equivalent band from a *ΔmxiC* "+ CR" sample was analysed in parallel: again, IpgB1 was the top T3S-related hit (32). The *mxiCV256P* mutant also leaked MxiC at wild-type levels and other effector proteins, although less than *ΔmxiC*. Its own inducible secretion was reduced and that of all translocators slightly affected (Fig. 5D). These results suggest that a "straightened" MxiC favours the earliest step in the induction hierarchy, i.e. IpaD secretion, whilst a "bent" MxiC can not prevent or favours, independently of its own secretion, the final one, i.e. effector release. In the wobbly mutant, three residues are altered that are initially identical to those changed in the straight one but its phenotype is opposite, i.e. more like the bent one. This indicates that it is not the chemical nature of the amino acids in this surface patch that leads to these phenotypes, but rather the stability of the secondary structure they form.

MxiC is not in its "straight" conformation in solution

The secretion patterns observed in the helix 9 mutants suggested movement in this area of MxiC is required for its function. We decided to examine the molecular conformation(s) of MxiC using double electron-electron resonance (DEER), also known as pulsed electron double resonance (PELDOR). This an increasingly popular electron paramagnetic resonance (EPR) technique used to measure distances between paramagnetic spin labels on a nanometre-scale (reviewed in (52)).

Based on the MxiC structure (chain A of PDB entry 2VJ4; (21)) and the "bent" model (supplemental Fig. S8A), we chose residues A247 and S290 to introduce paramagnetic centres into the molecule as the distance between these residues was predicted to be in the measurable range for both forms and the difference in distance between both forms was predicted as significant enough to be detectable (supplemental Fig. S9). To covalently couple the paramagnetic nitroxide label MTSL to these residues, A247 and S290 were mutated into cysteines. At the same time, the two endogenous cysteines C184 and C233 were mutated into alanine and serine, respectively, to finally generate a quadruple mutant *mxiC(C184A,C233S,A247C,S290C)* or *mxiC(Cys)*. Alternative, complementary mutant MxiCs, with cysteines for labelling inserted at two sets of different but equally suitable locations, could not be purified in sufficient amounts (not shown).

mxiC(Cys) behaved like the complemented strain in a CR secretion assay (supplemental Fig.

S10). A His-tagged version of the cysteine mutant (His-MxiC(Cys)) was soluble when expressed in *E. coli* (supplemental Fig. S11A). We also combined the quadruple cysteine mutant with the previously generated "bent" (*mxiCV256P*) and "straight" (*mxiC(I251A,T253A,S254A,D255E)*) mutants. However, neither His-MxiC(bent,Cys) nor His-MxiC(straight,Cys) were solubly expressed in *E. coli* (not shown). Thus, we could only analyse the "wild-type" His-MxiC(Cys).

MTSL was covalently coupled to His-MxiC(Cys) at residues 247 and 290. The protein was concentrated and mixed with deuterated glycerol for EPR/DEER experiments (for details see Experimental Procedures). First, the labelling efficiency was assessed using continuous wave room temperature EPR on a 35 µM sample (Fig. 6A). Using a previously obtained standard curve, the spin concentration was calculated to be 66 µM. The amount of residual unbound label was calculated to < 1%, thus a spin labelling efficiency of close to 100% could be extracted. The spectrum also indicated the protein was folded: because of increased mobility in a disordered structure, an unfolded protein would result in a spectrum similar to that of the free label.

We subsequently performed a DEER experiment to determine the distance distribution of the paramagnetic labels on C247 and C290. We obtained a distance distribution between 1.5 nm to 3 nm with two prominent peaks at 2 nm and 2.4 nm (Fig. 6B-C). Reliability of the two peaks comes from the high signal-to-noise F(t) trace. We simulated the expected distance distribution for the "bent" MxiC model (Fig. 6C) and the MxiC structure (PDB code 2VJ4, chain A; Fig. 6B) using MMM (35) and found the experimental data obtained for labelled His-MxiC(Cys) fit neither simulation well (Fig. 6). The major distance peak for the straight MxiC structure was around 3 nm while in the "bent" MxiC model, the major expected distance is at ~ 1 nm. As the distance simulations depend on the orientation of the side-chains to calculate the probabilities of the label rotamers, we simulated the expected form factors and distances for all seven individual chains in the three MxiC crystal structures (PDB codes 2VIX, 2VJ4 and 2VJ5; (21), supplemental Fig. S12). While the modelled form factors all differ in their overall shapes, they all show distances in the 1.5 nm to 3 nm range, in line with the experimental set-up. However, the simulated peak at 3 nm was not as prominent in the experimental data. We thus conclude that the experimental data is consistent neither with the structures, nor with the bent model. When modelling the possible observable distances in the structure and the "bent" model using the "all rotamers" function in MMM (35), which neglects side-chain atoms, labelling of the chosen sites in both conformations can achieve a distribution close to the experimentally observed distribution (data not shown). Thus, the conformation(s) of purified MxiC in solution is consistent with both bent and straight forms.

IpaD interacts with MxiC in solution without altering its conformation

As EPR only detects signals from paramagnetic centres, one can add potential binding partners to the sample without affecting the signal as long as they are diamagnetic. To determine whether other T3S related proteins influence MxiC's conformation, we mixed labelled His-MxiC(Cys) with a ten-fold molar excess of the proposed interaction partner IpaD (15) or of Spa15 (supplemental Fig. S11B), a protein that is not known to interact with MxiC (23). Spa15 addition did not change the continuous wave EPR spectrum (Fig. 7A), indicating Spa15 does not influence the rotational freedom of the labels in MxiC. Consistently, the DEER form factor and resulting distance distribution were also unchanged (not shown). Thus, Spa15 does not affect MxiC's conformation *in vitro*.

In contrast, addition of a 10-fold molar excess of purified His-IpaD (supplemental Fig. S11C) changed the continuous wave (cw) spectrum obtained (Fig. 7C), indicating the conformational freedom of the spin-labelled side chains has been affected by IpaD-MxiC complex formation, either due to direct interaction with IpaD residues or to subsequent conformational changes in MxiC. To confirm IpaD was responsible for signal modification, we mixed MxiC with different concentrations of IpaD (Fig. 8D). We found that the larger the stoichiometric fold of IpaD vs MxiC, the bigger was the spectral change detected. This shows the signal modification is specific to IpaD addition and that, in the concentration range used, we can modify the ratio of MxiC-IpaD complex vs MxiC alone in the

equilibrium ensemble. We also diluted the 10:1 IpaD-MxiC mix 1:4 (Fig. 7E). This confirmed that in preventing the interaction between MxiC and IpaD by dilution, the MxiC alone signal is recovered, meaning the interaction is reversible.

Given the evidence that MxiC family proteins can interact directly with translocator chaperones (27,36-38), we also purified the IpgC dimer and an IpaC-IpgC 1:1 heterocomplex ((39); supplemental Fig. S11D). Neither of these, added at 10-fold molar excesses, interacted with MxiC, alone (Fig. 7B) or when added in the presence of a 10-fold molar excess of IpaD (Fig. 7C). Taken together, these data indicate that in solution only IpaD displays an affinity for MxiC. However, we found no evidence of a distance change between the two spin labelled side chains by DEER upon addition of any protein partners (data not shown).

mxiC mutants unable to prevent effector secretion are affected differentially by needle mutant mxiHK69A, which is unable to release MxiC and hence effectors

To dissect at which point they are deregulated, we wanted to understand whether our *mxiC* mutants that leak effectors do so because MxiC's function(s) in blocking effector secretion is compromised or because they can not retain MxiC intracellularly. We examined this by combining them with a mutation that prevents MxiC secretion, *mxiHK69A*.

A *mxiHK69A* mutant in the needle protein does not secrete effector proteins (16) or MxiC secretion (12). However, a *mxiHK69A* mutant lacking MxiC (*ΔmxiHΔmxiC*/*mxiHK69A*) can secrete effectors (12). Thus, *mxiHK69A* does not physically block effector secretion, but it is unable to release MxiC's block of effector secretion.

When combining our *mxiC* mutants with *mxiHK69A*, MxiC mutants that cannot prevent secretion because the mutation(s) is affecting function should continue to leak effectors even if MxiC is retained inside bacteria. For instance, the hydrophobic core *mxiCF206S* mutant (Fig. 1) analysed by Cherradi et al. (2013) is not secreted in a *mxiHK69A* background, but still unable to block effector secretion. This indicates it has a severe defect in its inhibitory function that is independent of MxiC secretion (33). On the other hand, mutants where MxiC is functional but is secreted prematurely should prevent effector secretion when MxiC is forced to remain intracellular. To test this, we generated *mxiH* and *mxiHK69A* plasmids compatible with our *mxiC* mutant ones, which were then co-transformed into *ΔmxiCΔmxiH* (see Experimental Procedures). We focused solely on MxiC mutants displaying premature secretion of effectors and MxiC leakage. For completeness, we included also *mxiC(E201K,E276K,E293)*, which carries mutations in a negatively charged surface patch (Fig. 1A), secretes translocators and MxiC prematurely and is defective in IpaD secretion upon activation (15).

We were unable to detect leakage from *ΔmxiCΔmxiH*/*mxiCmxiH* (not shown) and its inducible secretion was also slightly reduced compared to wild-type but of similar level to that of *ΔmxiCΔmxiH*/*mxiCmxiHK69A* (Fig. 8, *top panels*). Indeed, slightly fewer functionally mature T3SSs are assembled in *ΔmxiH*/*mxiHK69A* relative to wild-type (16). However, as expected, *ΔmxiCΔmxiH/mxiCmxiHK69A* could not leak or induce secretion of the effectors IpaA or IpgD, nor of MxiC (Fig. 8, *bottom panels*), respectively. Yet, it secreted slightly reduced amounts of the translocators inducibly, as previously observed (16). In *ΔmxiCΔmxiH/mxiHK69A,* IpaA and IpgD leakage was restored and their secretion was also partially inducible (Fig. 8, *bottom panel*). We then examined how each *mxiC* mutant behaved in an *mxiHK69A* background. We focused on leakage in the absence of induction since activation of MxiC secretion is blocked in a *mxiHK69A* background but effector secretion might be allowed by a functionally defective MxiC.

Only *mxiCK68E* was unable to leak or induce effector secretion in the presence of *mxiHK69A* but not of *mxiH*. This indicates it is the only mutant where MxiC would be functional in blocking effector secretion, if it were not secreted prematurely. All other mutants leak effectors similarly whether *mxiH* or *mxiHK69A* is present, indicating that in these mutants MxiC's function(s) in blocking effector secretion are affected, either directly as in *mxiC(M226K,L242D)* or indirectly, via premature secretion of translocators as in *mxiC(E201K,E276K, E293)*.

DISCUSSION

Classes of mxiC mutants

Our mutants can be organised into classes according to their phenotypes (Table 1). However, residues mutated in the different classes do not obviously cluster in specific regions of the molecule (Fig. 1). Moreover, none seems affected only in a single step, i.e. regulation of translocator, MxiC or effector secretion. This indicates the three regulatory functions of MxiC are interlinked. Therefore, the mutants were classified according to where their main initial defect lies, assuming the regulatory steps occur in this order.

Only one mutant showed such severe loss-of-function as to resemble *ΔmxiC*: *mxiCΔCterm,* which we therefore placed in Class 0. However, unlike *mxiCΔCterm*, *mxiCΔNterm* and *mxiCΔCBD* were still largely able to induce translocator –but not MxiC– secretion, suggesting they are not full loss-of-function mutants (Class 1a). Mutant *mxiCV256P* also could not secrete MxiC well inducibly or in a *ΔipaB* background, suggesting it has some defect in MxiC secretion. This mutant leaks effectors but as it can still stimulate secretion of translocators, it is also not a complete loss-of-function mutant (Class 1a). Both classes of mutants readily by-passed the block on effector secretion imposed by *mxiHK69A* although none secreted MxiC efficiently in this background, indicating they are unable to establish all or some of MxiC's regulatory functions.

mxiCK66E and *mxiCK68E* are phenotypically similar in that they secrete MxiC prematurely, and hence show reduced translocator induction and increased effector leakage. However, MxiCK68E is secreted much more efficiently than MxiCK66E. Furthermore, amongst all mutants, only MxiCK68E does not leak effectors in a *mxiHK69A* background. This indicates that the mutations in MxiCK68E and MxiCK66E, despite their proximity and chemical similarity, lead to different defects. K68E (Class 1c) primarily deregulates MxiC secretion, leading it and effectors to be secreted prematurely. On the other hand, in addition to some premature secretion, K66E (Class 1b) seems to confer more fundamental defect(s) leading to effector leakage. Finally, the only defect seen in *mxiC(M226K,L242D)* is effector leakage (Class 1d).

Class 2 mutants are primarily, if oppositely, affected in translocator release: MxiC(E201K,E276K,E293) can not induce IpaD secretion but leaks IpaB, IpaC, itself and effectors (15), while MxiC (I251A,T253A,S254A, D255E) displays increased IpaD secretion and reduced IpaB and IpaC secretion.

Properties of MxiC and roles of its termini

Using the mutant classes, we conclude that several physiological features of MxiC are regulated: 1) its secretion, since several mutants up- or downregulate it; 2) hierarchical secretion of translocators and effectors, and even of proteins within those two categories; 3) the ability to switch from translocator to effector secretion. There are also uncharacterised fundamental properties of MxiC as indicated by mutations that most likely do not affect its overall structure, i.e. *mxiCΔCterm* and *mxiCΔNterm*, but still lead to full or partial null phenotypes, respectively.

That MxiC's secretion signal and putative CBD are dispensible for stimulation of translocator secretion indicate Domains 1-3 alone mediate this function. Multiple residues in the C-terminal helix of MxiC are highly conserved. Schubot et al. (2005) suggested that the C-terminal helix of *Yersinia* TyeA (a MxiC domain 3 homolog which binds the C-terminus of YopN, a MxiC domains 1-2 homolog) might localise the YopN/TyeA complex to the secretion apparatus. Ferracci et al. (2005) found TyeA to be essential for YopN to block secretion. In addition, several mutants in the hydrophobic core of domain 2 (Fig. 1) of MxiC are non-functional or at least unable to block secretion (33). In contrast, equivalent mutations in *Yersinia yopN* lead to a general block of secretion (19,33). However, the *yopN* mutants analysed by Ferracci et al. (2005) were overexpressed in comparison to wild-type levels. In our hands, overexpression of the non-functional hydrophobic core of domain 2 *mxiCD225V* mutant (Fig. 1) also led to a general block of secretion (not shown). This suggests MxiC blocks an acceptor site on the secretion apparatus and too much non-removable protein prevents release of this repressor, consequently blocking secretion. In support of this, Lee et al (2014) showed Pcr1, the *Pseudonomas* T3SS homologs of *Yersinia* TyeA, interacts with the T3SS inner membrane protein

PcrD, known as MxiA in *Shigella* (40). Furthermore, the extreme C-terminus of MxiC is required for interaction with the cytoplasmic region of MxiA (41), explaining the null phenotype of *mxiCΔCterm*. As mutants in the N-terminus and CBD are unable to secrete MxiC inducibly and an N-terminal His-tag on MxiC led to a *ΔmxiC* phenotype (data not shown), these regions may also be involved in binding it to and releasing it from that site.

MxiC differentially affects secretion of IpaD and hydrophobic translocators

Translocator secretion was largely unaffected in Class 1a and 1d mutants whilst all had clear defects in blocking effector secretion. In contrast, mutants from Class 2 modulated translocator secretion, but effector secretion was affected indirectly (*mxiC(E201K,E276K,E293K)*) or not at all (*mxiC(I251A,T253A,S254A, D255E)*). Thus, the action of MxiC on translocators and effectors can be uncoupled. MxiC(E201K,E276K,E293K) acts as if it had already received the activation signal (15). Thus, MxiC's action on translocators can also be uncoupled from the needle-transmitted activation signal. In addition, MxiC secretion is not required for activating translocator secretion, as a *mxiHK69A* mutant –which does not secrete MxiC– and *mxiCΔNterm* secrete normal levels of translocators (12,16).

Even hydrophilic versus hydrophobic translocator secretion can be uncoupled since *mxiC(E201K,E276K,E293K)* leaks IpaB and IpaC and is unable to induce IpaD secretion (Roehrich et al. 2013). Interestingly, the "straight" mutant *mxiC(I251A,T253A,S254A,D255E)* instead displays reduced induction of IpaB and IpaC, while IpaD secretion is slightly increased. These opposite effects correlate with the mutations being on opposite faces of MxiC (Fig. 1, *top*). These faces are also the ones that may undergo a conformational change from flat to bent (21). In fact, this is the conformational change we tried to prevent in *mxiC(I251A,T253A,S254A,D255E)*. Furthermore, the predicted "bent" mutant (*mxiCV256P*) and the predicted "straight" mutant show opposite phenotypes: while the former leaks effectors and is only weakly affected in translocator secretion, the latter shows differential induction of translocators. Thus, reduced secretion of the repressor IpaD could affect secretion of the hydrophobic translocators. Alternatively or additionally, MxiCV256P was only poorly secretable and could be affected in more fundamental functions. While we cannot exclude that these mutations mainly affect MxiC interactions by altering its surface, the type of mutations, the fact that the mutations are directly adjacent and their opposite phenotypes suggest that we have modified MxiC's ability to undergo conformational changes.

A conformational change in MxiC?

The negatively charged patch mutated in *mxiC(E201K,E276K,E293K)* lies on the face of the molecule that is flat in MxiC, but concave in YopN/TyeA and the *E.coli* homolog SepL (26). As the "straight" mutant favoured IpaD secretion, a flat negatively charged patch might be required for this. Lower levels of IpaB and IpaC secretion could then be due to the restricted conformation or to the mutations themselves. In other words, IpaB and IpaC secretion could require either a bent conformation or the area in helix 9 that was mutated in *mxiC(I251A,T253A,S254A, D255E)*, or both. The latter is supported by the work of Archuleta et al. (2014), which indicates that a flattened gate-keeper structure has a conserved binding site for translocator chaperones, such as IpgC in *Shigella*, at this location (27). In the *Salmonella* SPI-1 system, the MxiC homologue InvE interacts with complexes of hydrophobic translocators and their chaperone (36). An interaction between MxiC or its homologue and the class 2 chaperone IpgC or its homologue has also been shown in *Shigella* and *Chlamydia* (33,38). Finally, we identified substoichiometric amounts of IpgC and all translocators in our interaction partner screen (32).

MxiC directly interacts with IpaD

Unfortunately, we were to unable to test for any conformational change in MxiC by EPR. However, we did detect an interaction between MxiC and IpaD via this method. The spectral changes observed in the continuous wave EPR experiments where MxiC(Cys) and IpaD were mixed have two possible explanations: i) the increased molecular weight of the complex(es), which is reflected in slower overall rotational correlation times; ii) a direct interaction between

the spin-labelled probes and residues in IpaD. While the reason of the spectral effects observed cannot be clarified, it corroborates the notion that complex formation between MxiC and IpaD occurs. From Fig. 7B, assuming the 1:10 MxiC:IpaD concentration corresponds to the maximum amount of complex formation and therefore that a 1:5 molar ratio IpaD gives half maximum complex concentration, we estimate the dissociation constant of the MxiC-IpaD complex is ~730 µM, i.e. these purified proteins have very low affinity. This suggests we have not fully reconstituted interactions between these proteins *in vitro*. We may be lacking their "scaffold". Perhaps the $MxiA_C$ oligomer, aided by other T3SS export apparatus components, stabilises one of MxiC's conformations?

Based on the crystal structures of IpaD (42) and MxiC (21) and the mutations genetically affecting the interaction between these proteins (*ipaDL99P* and *mxiC(E201K,E276K,E293K*); (15)), we built a model of the MxiC/IpaD interaction: the MxiC and IpaD structures pack readily against each other (Fig. 9A), with the negatively charged patch of MxiC (E201, E276 and E293) at their interface, yielding an overall elongated form. The interacting surface is relatively flat, contains several charged residues on the edges and stacked tyrosine residues in the centre giving an interface formed by two charge-complementary surfaces (Fig. 9B). This model is consistent with the data of Lee et al. (2014), who found that *Pseudomonas* PcrG, a homolog of the N-terminus of IpaD, interacts with Pcr1, a MxiC domain 3 homolog (40). Taken together with the work of Archuleta et al. (2014) (27), our model suggests why MxiC's N-term and CBD are dispensible for stimulating translocator secretion.

Intramolecular and external signals for MxiC secretion

By analysing the *mxiCΔNterm* mutation in the constitutive secreter background *ΔipaB* we confirmed that this mutant is unsecretable. Similar to the N-terminal secretion signal, the putative chaperone-binding domain is required for efficient MxiC secretion. However, this domain did not affect secretability. Thus, MxiC secretion is merely deregulated in *mxiCΔCBD*. Interestingly, two different mutations in the CBD of MxiC led to increased MxiC leakage: *mxiCK68E* and *mxiCK66E*. Taken together, these data suggest that the putative chaperone-binding domain positively regulates MxiC secretion.

That the chaperone-binding domain is irrelevant for MxiC secretion in the *ΔipaB* background is reminiscent of the lack of requirement of MxiC for translocator secretion in the same background. Similar to the repression of translocator secretion (12), an intracellular repressor mechanism for MxiC secretion might be put into place once the tip is fully assembled: the CBD would be involved in counteracting this mechanism and mutants *mxiCK68E* and *mxiCK66E* would then either be better at counteracting the mechanism repressing MxiC secretion or less sensitive to it.

The "external" signal for MxiC secretion has not yet been identified. However, this signal is likely transmitted through the needle as a *mxiHK69A* mutant is unable to release MxiC even when secretion is artificially activated by additional deletion of *ipaB* (12). The question of how *mxiHK69A* blocks MxiC secretion remains: the *mxiHK69A* mutant is either unable to transmit an external activation signal for MxiC secretion generated after the translocators have been secreted, or this mutation alters the affinity of the secretion apparatus for MxiC (12,32).

Mutants *mxiCK68E* and *mxiCK66E* leaked the respective mutant protein and hence probably overcome an intracellular repression mechanism for MxiC secretion. Similarly, *mxiC(E201K,E276K,E293K)* has gained the ability to activate its own secretion (15). However, none of these mutants is inducibly secreted in the *mxiHK69A* background. Indeed, we did not identify any mutation allowing induction of MxiC secretion in the *mxiHK69A* background. Thus, in addition to blocked transmission of Signal 2, the secretion apparatus in the *mxiHK69A* mutant is unable to release/recognise MxiC as a secretion substrate.

MxiC secretion per se is not required to derepress effector secretion

In the wild-type, the needle transmits the activation signal to MxiC, whose subsequent secretion leads to derepression of effector secretion. Classe 1a mutants, which only secrete

MxiC poorly, but leak effectors, show that effector secretion and MxiC secretion can also be uncoupled. In other words, MxiC secretion *per se* is not required for allowing effector secretion. Not all MxiC homologues are secreted (28). However, the gate-keepers must be removed from their initial place of action: in the *Salmonella* SPI-2 system where the MxiC homologue SsaL is not secreted, the protein dissociates from the membrane and is degraded once secretion is activated (43).

Further regulatory function(s) for MxiC?

Mutant *mxiCV256P* leaked effectors, but specifically high levels of IpgB1. IpgB1 is an effector protein chaperoned by Spa15 (24,44). The specific effect of *mxiCV256P* on IpgB1 suggests that MxiC somehow directly affects secretion of at least some effectors. Similarly, *E. coli* SepL was shown to specifically act on the effector Tir. This protein-protein interaction was proposed to be critical for regulating secretion of the other effector proteins (28). Though this does not exclude a possible effect of MxiC on effector secretion in a more general way, e.g. by modulating the affinity or physically blocking an acceptor site for effectors in the T3SS, it suggests that secretion of specific effectors involves an additional regulatory layer.

Steps in MxiC function

After T3SS assembly, but prior to secretion activation, multiple mechanisms are in place that prevent premature secretion of the different protein types. Translocator secretion is repressed by IpaD, probably via interaction with MxiC bound to MxiA. An uncharacterised mechanism prevents MxiC secretion, while this protein itself prevents effector secretion. When the needle tip comes in contact with a host cell, an activation signal ("Signal 1") is transmitted to the cytoplasm, most likely through the needle.

The mechanism preventing premature translocator secretion is counteracted by MxiC. Secretion of IpaD requires the negatively charged patch and probably a flat conformation of the molecule. Removal of IpaD may initiate a conformational change in MxiC, which bends to release the IpgC chaperone and its bound translocators allowing these to become secreted in turn. IpaB and secreted IpaC form a pore, connected to IpaD at the needle tip and also inserted in the host cell membrane, which transmits "Signal 2" to the cytoplasm. Reception of this signal may allow finalisation of a conformational change in MxiC that releases it for secretion. Then, early effectors are secreted. Moreover, as both negative regulators are now removed, the secretion rate is enhanced (40), possibly through alteration of its mode (41).

By using structure- and sequence based mutagenesis of *mxiC*, we dissected at which stages of the regulatory cascade MxiC acts with which function and which steps can be uncoupled. This also allowed us to determine how the different steps are connected. Finally, we provide the first evidence that directionally defined conformational change in MxiC is involved in controlling the secretion hierarchy. The conservation of the components involved indicates the importance of this regulatory pathway to T3SS-carrying bacterial pathogens of animals.

EXPERIMENTAL PROCEDURES

Bacterial strains, plasmids and primers

Supplemental Tables S1 and S2 list the strains and plasmids used. *S. flexneri* strains were grown in Trypticase Soy Broth (Becton Dickinson) at 37°C with appropriate antibiotics at following final concentrations: ampicillin 100 µg ml-1, kanamycin 50 µg ml-1, tetracycline 5 µg ml-1, chloramphenicol 10 µg ml-1. IPTG was used at the final concentrations indicated in the Fig. Legends. Supplemental Table S3 lists the primers used.

Construction of plasmids

Plasmids were generated as described below and verified by sequencing.

pIMA221 (pWSK29**mxiC*) was generated by amplifying *mxiC* from the *Shigella* virulence plasmid pWR100 using primers mxiC_SacI and mxiC_BamHI. The purified PCR product was digested with SacI and BamHI and cloned into pWSK29* (modified pWSK29 (45) lacking the T7 promoter, a gift from Andrew Davidson (University of Bristol) digested with the same enzymes.

Terminal deletions and mutations. To express the terminal *mxiC* deletions, *mxiC* was amplified from pIMA221 using primers mxiC_SacI_del30 and mxiC_BamHI for *mxiCΔNterm*, primers mxiC_SacI and mxiC_341 for *mxiC(1-341)*. The resulting PCR products were digested with SacI and BamHI. Fragments *mxiCΔNterm* and *mxiC(1-341)* were cloned into pACT3 digested with SacI/BamHI yielding pDR60 and pDR73, respectively.

Chaperone binding domain mutants. pDR80 contains *mxiCΔCBD*, an internal deletion mutant that was created by two step PCR and lacks residues 32 to 72. The *mxiC* gene was amplified from pIMA208 using primer pairs mxiC_SacI/mxiC_D32-72_R and mxiC_D32-72_F/mxiC_BamHI. The obtained PCR fragments were used as template for the second PCR step using primers mxiC_SacI and mxiC_BamHI. The PCR product was purified, digested with SacI/BamHI and ligated into pACT3 digested with the same enzymes.

Mutant *mxiCK66E* was generated by two-step PCR. First, *mxiC* was amplified from pIMA208 using primers mxiC_SacI and mxiC_K66E_R and or mxiC_K66E_F and mxiC_BamHI, respectively. These fragments were combined and reamplified using mxiC_SacI and mxiC_BamHI. The PCR products were purified, digested with SacI and BamHI and cloned into pACT3 digested with the same enzymes yielding pDR96. pDR100 contains *mxiCK68E* cloned via SacI/BamHI, equivalent to amplification of mutant *mxiC* using primers mxiC_SacI and mxiC_BamHI. This mutant was obtained by chance and retained as the mutation was in a relevant area of the molecule.

Hydrophobic patch mutant. Double mutant *mxiC(M226K,L242D)* was generated by two-step PCR. First, pIMA212 was used as template for reactions with primer pairs mxiC_SacI/mxiC_M226K_R and mxiC_L242D_F/mxiC_BamHI. The obtained fragments were combined and reamplified using primers mxiC_SacI and mxiC_BamHI. The product was purified, digested with SacI and BamHI and cloned into pACT3 digested with the same enzymes, yielding pDR72.

Hinge region mutants. Mutants in helix 9 were generated by two-step PCR: first, mxiC was amplified from pIMA208 using primer pairs mxiC_SacI/mxiC_V256P_R, mxiC_V256P_F/mxiC_BamHI, mxiC_SacI/mxiC_wobble_R, mxiC_wobble_F/mxiC_BamHI, mxiC_SacI/mxiC_straight_R2, mxiC_straight_F2/mxiC_BamHI. The obtained PCR fragments were used as template for the second PCR using primers mxiC_SacI and mxiC_BamHI. The products were purified and digested with SacI/BamHI before ligation into pACT3 digested with the same enzymes. The resulting plasmids were named pDR91 (pACT3mxiCV256P), pDR92 (pACT3mxiC(T253G,S254G,D255G)) and pDR93(pACT3mxiC(I251A,T253A,S254A,D255E)), respectively. The background quadruple cysteine mutant gene *mxiC(Cys)* (Cys184Ala (TGT to GCA), Cys233Ser (TGT to TCT), Ala247Cys (GCA to TGT), Ser290Cys (AGT to TGT)) required for EPR experiments was synthesised by MWG Eurofins and supplied as pEXA-mxiC_EPR2. For pDR104 (pET28b*mxiC(Cys)*), *mxiC(Cys)* was amplified from the pEX-A-mxiC_EPR2 using primers mxiC_NdeI_F/mxiC_EcoRI_R. The PCR product was purified and digested with NdeI/EcoRI before cloning into pET28b (Novagen).

Chaperone mutants

Deletions of the chaperone genes were performed using the method of Datsenko and Wanner (46). A kanamycin cassette was amplified from pKD4 using primers ipgA_KO_kanF/ipgA_KO_kanR, ipgE_KO_kanF/ipgE_KO_kanR and spa15_KO_kanF/spa15_KO_kanR, respectively. The primers contained ca. 50 bp upstream and downstream of the respective chaperone gene to allow for recombination by the λ Red recombinase. These fragments were introduced into Shigella wild-type yielding ΔipgA, ΔipgE and Δspa15, respectively. For ΔipgE Δspa15 (abbreviation of ΔipgE::FRT Δspa15::kan) and ΔipgE ΔipgA (abbreviation of ΔipgE::FRT ΔipgA::kan), the kanamycin cassette was removed in ΔipgE by FLP mediated recombination using the introduced FRT sites yielding ΔipgE::FRT. The same fragments used for the deletion of spa15

and ipgA in the wild-type background were now used for λ Red recombination in ΔipgE::FRT. This step was of low efficiency as the recombination preferentially occurred at the FRT scar at the ΔipgE site and not up- and downstream of spa15 and ipgA, respectively. Colonies were prescreened by colony PCR using primers annealing ca. 200 bp to 300 bp upstream and downstream of the original chaperone gene, seeking to obtain a PCR fragment with a size compatible with the insertion of the kanamycin cassette versus the chaperone gene. ΔipgE ΔipgA Δspa15 (abbreviation of ΔipgE::FRT ΔipgA::FRT Δspa15::kan) was generated by removing the kanamycin cassette in ΔipgE ΔipgA by FLP recombination yielding ΔipgE::FRT ΔipgA::FRT and subsequent λ Red recombination using the ipgA::kan PCR fragment. Again, this step was of low efficiency as now two FRT sites were available on the virulence plasmid and colonies were prescreened by colony PCR as described for the double knockouts. All insertions and cassette removals were verified by sequencing.

Combination of mxiC and mxiH mutants

Some of the mxiC plasmids detailed above were then combined with plasmids carrying mxiHK69A, or wild-type mxiH as control in ΔmxiCΔmxiH (12). mxiH and mxiHK69A were amplified from corresponding templates (16) using primers mxiH_NdeI_For and mxiH_PstI_Rev, and cloned into a previously described pUC18 vector, modified to carry a constitutive lac operator (14). This was done so when both pACT3 containing mxiC and pUC18 containing mxiH were transformed into ΔmxiCΔmxiH bacteria, mxiH expression would not be inhibited by LacI, encoded on pACT3, binding to the lac operator of pUC18. The corresponding bacteria had normal expression of mxiH and mxiC in the presence of 25 µM IPTG except ΔmxiCΔmxiH/mxiCΔNterm mxiH wild-type or K69A when 100 µM IPTG was used to ensure sufficient expression of this mxiC mutant.

Type III secretion functional assays

Analysis of protein expression levels. Whole cultures of *S. flexneri* in late exponential phase (OD_{600} ca. 1) were mixed with 4x Laemmli sample buffer ("whole culture lysates"). Samples from equivalent cell numbers (ca. 3 x 10^6 cfu) were separated by 10% SDS-PAGE and immunoblotted.

Analysis of leakage. *S. flexneri* strains grown to OD_{600} ca. 1 were collected by centrifugation at 15900 g for 10 min at 4°C. The supernatants were mixed with 4x Laemmli sample buffer, normalised for equivalent cell numbers, separated on 10% SDS-PAGE and visualised by silver staining or immunoblotting. On silver stained SDS-PAGE, labels indicate the position of proteins as determined by mass spectrometry or from deletion strains.

Analysis of inducible protein secretion. Congo red (CR), a small amphipatic dye molecule, is an artificial inducer of T3S. Its addition to a *Shigella* culture leads to a burst of Ipa protein secretion called "induction" (47,48). *S. flexneri* at OD_{600} ca. 1 were collected by centrifugation at 4500 g and resuspended in PBS to an OD_{600} of 5, i.e. ca. 1.5 x 10^9 cfu ml^{-1}. For each strain, two reaction tubes were prepared with 500 µl bacterial suspension. To one of the tubes, CR (Serva) was added to a final concentration of 200 µg ml^{-1}. After incubation at 37°C for 15 min, samples were centrifuged at 15900 g for 10 min at 4°C. 20 µl of the supernatants denatured in Laemmli sample buffer were subjected to 10% SDS-PAGE and visualised by silver staining or immunoblotting.

Western blotting

Proteins were transferred onto Immobilon FL (Millipore) membrane using a semi-dry method. Primary antibodies used were: anti-IpaA mouse monoclonal, gift from Kirsten Niebuhr (3); anti-IpaB mouse monoclonal, named H16, gift from Armelle Phalipon (49); anti-IpaC mouse monoclonal, mixture of J22 and K24, gift from Armelle Phalipon (50) anti-IpaD rabbit polyclonal, gift from Claude Parsot (51) or as described in Cheung et al. (2015); anti-IpgD mouse monoclonal, gift from Kirsten Niebuhr (3); anti-MxiC rabbit polyclonal, raised against a fragment of MxiC containing residues 74 to 355 and an N-terminal His-tag (12). Near-infrared fluorescent secondary antibodies (rabbit IgG raised in goat

and coupled to Alexa680, Invitrogen; mouse IgG raised in goat and coupled to DyLight800, Pierce) were visualised and quantified on a Li-Cor Odyssey imaging system.

Calculation of the secreted percentage of a protein

Wild-type *Shigella* were grown to OD_{600} ca.1 and resuspended in PBS to an OD_{600} of 15. The suspension was brought to 37°C in a waterbath before CR was added at a final concentration of 200 µg ml-1 and the cultures were incubated for 8 min. For secreted proteins, samples were centrifuged at 15 000 g for 10 min at 4°C and supernatants were denatured in Laemmli sample buffer. For whole cultures, the bacterial suspension was directly denatured in sample buffer. To calculate the secreted percentage of each protein, we compared protein amounts in supernatants and whole cultures by Western blotting. Undiluted and 1:4 diluted supernatant was compared to a dilution series of the whole cultures. Near-infrared fluorescent secondary antibodies were quantified on a Li-Cor Odyssey imaging system. A linear fit of the dilution series allowed us to determine the concentration of protein in the supernatant in comparison to the whole culture.

EPR spectroscopy

Modelling of the bent MxiC structure. To create a model of the putative bent form of MxiC, its straight crystal structure (PDB code 2VJ4, (21)) and the structure of YopN/TyeA (PDB code 1XL3, Schubot et al. (2005)) were used. In a first step, MxiC was superimposed on YopN and TyeA independently. The majority of the first two X-bundle domains of MxiC (residues 64 to 253) were matched to YopN and the C-terminal domain of MxiC (residues 254 to 355) was matched to TyeA. Then the respective MxiC domains were taken and the link between them (residues 250 to 260) was rebuilt manually, guided by the conformation of the equivalent region in YopN. This model was soaked in a 1 nm layer of water molecules and relaxed with 5000 steps of energy minimisation under the Cvff forcefield. Insight II 2005 was used for the modelling and Discover 2.98 (both Accelrys Inc.) for the energy calculations.

Modelling of interspin distances. The spin label MTSL ((1-oxyl-2,2,5,5-tetramethylpyrroline-3-methyl)methanethiosulfonate; Berliner et al. (1982)) is relatively long and flexible: the linker to the protein backbone contains five dihedral angles. Thus, depending on the rotameric state of each spin label in a protein, the interspin distance can vary significantly. When bound to a protein, the spin label's rotamers have different energies due to their interactions with the neighbouring side-chains of the protein. The most favourable rotamers and thus the most likely distance distribution were calculated using MMM version 2013, a Matlab package ((35), http://www.epr.ethz.ch/software/index). We used eight different MxiC structures to calculate the interspin distance distribution: the "bent" MxiC model and all seven MxiC crystal structures from Deane et al. (2008) (PDB codes 2VIX, 2VJ4 and 2VJ5) were extracted so that only a single polypeptide chain was present in each PDB-file. This was necessary as the labelled residues (247 and 290) are in close proximity to the other polypeptide chains in the original PDB files. The neighbouring chains thus also influence the rotamer modelling, however, MxiC is most likely monomeric in solution (21) thus these additional interactions are not meaningful and were excluded.

Protein purification. Each protein was purified firstly by Nickel affinity chromatography and then by size-exclusion chromatography. The protocols for these purifications were based on articles herewith: Spa15 (53), IpgC/IpaC (39), MxiC(C184A/C233S/S243C/S290C) (21). For IpaD, a C322S mutant was used to avoid the requirement for DTT addition during the purification (54). For this, His6-$IpaD_{15\text{-}332\ C322S}$ was amplified from pUC18 $ipaD_{C322S}$ (14) using primers ipaD15_NdeI_For and ipaD_BamHI_Rev (supplemental Table S3), and cloned into pET15b (Novagen) via NdeI/BamHI. The changes to the protocol for each protein are detailed in supplemental Table S4.

All protein concentrations, measured with a Nanodrop Lite Spectrophotometer (Thermo Scientific), were adjusted using molecular weight, extinction coefficient (as obtained from the Expasy server) of the protein and considering also

the path length. Prior to each protein purification, the appropriate bacterial strain was streaked out on an Lysogeny Broth (LB) agar plate containing the appropriate antibiotics and grown overnight at 37 °C. The next day small LB cultures were made overnight. In the morning, cultures were made with overnight cultures (supplemental Table S4). Bacteria were grown to an OD_{600} of ca. 0.6 before cooling to 20 °C and induction with a final concentration of 1 mM IPTG. Cultures were then left shaking at 20 °C overnight.

Cells were harvested by centrifugation (5000 g 15 minutes), washed in 10 ml PBS (3500 g rpm 15 min) and resuspended ca. 30 ml Binding buffer with protease inhibitors (Complete EDTA-free, Roche). Bacteria were lysed by sonication (Sonics Vibra cell™) amplitude 60 %, pulse 1 sec on 1 sec off, Time 30 sec and variable cycle numbers (supplemental Table S4).

Lysates were clarified by centrifugation for 30 min at 20000 g at 4 °C. Supernatants were filtered through a 0.45 µm and then 0.22 µm syringe filter (Sartorius) and applied to a 5 ml HisTrap FF column (GE Healthcare) equilibrated in binding buffer (supplemental Table S4) using a peristaltic pump (GE Healthcare). The entire supernatant was passed over the column three times at 2.5-5 ml/minute at 4 °C. The column was then connected to an ÄKTA (GE Healthcare) and washed with 10-15 column volumes of Binding buffer, followed by elution buffer (supplemental Table S4). Elution of bound proteins was carried out in the presence of protease inhibitors, with an imidazole gradient from 20 mM to 1 M (Elution buffer; supplemental Table S4) to 3 ml/min for 25 min. 5 ml fractions were collected. Peak fractions potentially containing proteins of interest had their concentration determined at A_{280} and were examined using Coomassie-stained SDS-PA gels. The appropriate fractions were pooled and concentrated using Amicon Ultra spin concentrator (Molecular cut off, Millipore; supplemental Table S4).

These concentrated fractions were run on a Superdex75 10/30 size exclusion chromatography column (GE Healthcare) equilibrated in 20 mM TrisHCl pH 7.5, 100 mM NaCl, 100-250 µl samples were applied and the column run at 0.5 ml/min collecting 1 ml fractions. Location and purity of proteins of interest was verified by Coomassie-stained SDS-PAGE. After the final gel filtration step, all samples were concentrated as above (supplemental Table S4) and flash frozen in aliquots in liquid nitrogen and stored at -80 °C until use.

MxiC labelling. 1 mM freshly made DTT (dithiothreitol; Sigma) was added to MxiC(C184A/C233S/A247C/S290C) to reduce the SH of the cysteines before concentration and application on the gel filtration column. The fractions containing His-MxiC(C184A/C233S/A247C/S290C) (ca. 2.12 mg/ml) were pooled and the spin label MTSL (1-oxyl-2,2,5,5-tetramethylpyrroline-3-methyl) methanethiosulfonate; Berliner et al., 1982; Toronto Research Chemicals, Toronto, Canada), was added at two-fold molar excess (ca. 121 µM). This means one molecule of MTSL was added per cysteine in the sample. After incubation for overnight at 4°C in the dark, the sample was concentrated to ca. 1.842 mM (~70 mg/ml) as determined by the A_{280} using Amicon Ultra-4 spin concentrators (10 kDa molecular weight cut off, Millipore).

Determination of the spin concentration and labelling efficiency using continuous wave EPR. To determine the labelling efficiency of His-MxiC(Cys) with MTSL, continuous wave EPR spectra were detected at room temperature on a E500 Elexsys Bruker spectrometer equipped with a super high Q cavity. The samples were thawed on ice and 20 µl were transferred into a 1.5 mm outer diameter glass capillary. A 14 mT field sweep was performed, with 0.15 mT modulation amplitude, 7.96 mW incident microwave power, ca. 9.38 GHz frequency. As the measured signal is the first derivative, the resulting curve has to be integrated to obtain the absorbance spectrum. Double integration yields the spin concentration as horizontal asymptote. The area under the absorbance spectrum is proportional to the spin concentration. The correlation factor was experimentally determined with a solution of known concentration of tempol in water.

Distance measurement using DEER. In this work the Q-band DEER experiments were performed as described in Polyhach et al. (2012).

By using deuterated cryoprotectants, the relaxation time can be increased thus increasing range of distance measurement and sensitivity. As protein samples are analysed at 50 K after flash-freezing in liquid nitrogen, the equilibrium population is observed, thus yielding a distance distribution rather than a single distance. For DEER, the sample was thawed on ice, 50 µl were transferred into a quartz tube (3mm outer diameter, Aachener Quarz-Glas Technologie Heinrich) and flash frozen in liquid nitrogen. Optimisation and evaluation of Q-band DEER experiments is described in Bordignon and Polyhach (2013). Data was acquired for 4 h to 12 h. Normalised experimental data (V(t)=V(0)) are background corrected to obtain the DEER form factor (F(t)=F(0)) by division by the background function (which is mainly due to intermolecular interactions). The form factor oscillates around a horizontal line at (1 - Δ) (Δ is the modulation depth) after background correction. The distance distribution is extracted from the form factor using DeerAnalysis2013 ((55), http://www.epr.ethz.ch/software/index).

Analysis of interactions between MxiC and other proteins using EPR. To analyse the interaction between MxiC and other proteins, we performed continuous wave X-band EPR spectroscopy at room temperature to detect eventual changes in the dynamic properties of the two spin labels on MxiC upon complex formation. Each EPR sample was prepared in gel filtration buffer (20 mM Tris-HCl pH 7.5, 100 mM NaCl), and contained a final concentration of ca. 75 µM of MxiC and 10 fold more of the other proteins (ca. 750 µM).

Acknowledgments: This work was supported by a studentship from the Centenary Postgraduate Fund at the University of Bristol to ADR, project grant WT088266 from the UK Wellcome Trust to AJB and IMA, project grant MR-J002097-1 from the UK Medical Research Council to AJB (supporting DS and MP), two short Master 1-level work-experience scholarships from the Université Pierre et Marie Curie (Paris 6) to SM. RBS thanks the Advanced Computing Research Centre at Bristol for provision of High Performance Computing and the University of Bristol for a Senior Research Fellowship. EB thanks the Freie Universität Berlin for supporting this research.

Conflict of interest: The authors declare that they have no conflicts of interest with the contents of this article.

Author contributions: ADR, EB, RBS, IMA and AJB conceived and designed the experiments; ADR, EB, SM, DKS, XL, MP, IM, RBS and AJB performed the experiments; ADR, EB, IMA, RBS and AJB analysed the data; XL and MP generated reagents and materials; ADR, EB, IMA, RBS and AJB contributed to the writing of the manuscript; all authors approved the final version of the manuscript.

REFERENCES

1. Kosek, M., Yori, P. P., and Olortegui, M. P. (2010) Shigellosis update: advancing antibiotic resistance, investment empowered vaccine development, and green bananas. *Curr Opin Infect Dis* **23**, 475-480
2. Hodgkinson, J. L., Horsley, A., Stabat, D., Simon, M., Johnson, S., da Fonseca, P. C., Morris, E. P., Wall, J. S., Lea, S. M., and Blocker, A. J. (2009) Three-dimensional reconstruction of the *Shigella* T3SS transmembrane regions reveals 12-fold symmetry and novel features throughout. *Nat Struct Mol Biol* **16**, 477-485
3. Blocker, A., Gounon, P., Larquet, E., Niebuhr, K., Cabiaux, V., Parsot, C., and Sansonetti, P. (1999) The tripartite type III secreton of Shigella flexneri inserts IpaB and IpaC into host membranes. *J Cell Biol* **147**, 683-693
4. Cordes, F. S., Komoriya, K., Larquet, E., Yang, S., Egelman, E. H., Blocker, A., and Lea, S. M. (2003) Helical structure of the needle of the type III secretion system of Shigella flexneri. *J Biol Chem* **278**, 17103-17107
5. Veenendaal, A. K., Hodgkinson, J. L., Schwarzer, L., Stabat, D., Zenk, S. F., and Blocker, A. J. (2007) The type III secretion system needle tip complex mediates host cell sensing and translocon insertion. *Mol Microbiol* **63**, 1719-1730
6. Roehrich, A. D., Martinez-Argudo, I., Johnson, S., Blocker, A. J., and Veenendaal, A. K. (2010) The extreme C terminus of Shigella flexneri IpaB is required for regulation of type III secretion, needle tip composition, and binding. *Infect Immun* **78**, 1682-1691
7. Shen, D. K., Saurya, S., Wagner, C., Nishioka, H., and Blocker, A. J. (2010) Domains of the Shigella flexneri type III secretion system IpaB protein involved in secretion regulation. *Infect Immun* **78**, 4999-5010
8. Menard, R., Sansonetti, P., Parsot, C., and Vasselon, T. (1994) Extracellular association and cytoplasmic partitioning of the IpaB and IpaC invasins of S. flexneri. *Cell* **79**, 515-525
9. Diepold, A., and Wagner, S. (2014) Assembly of the bacterial type III secretion machinery. *FEMS Microbiol Rev* **38**, 802-822
10. Brutinel, E. D., and Yahr, T. L. (2008) Control of gene expression by type III secretory activity. *Curr Opin Microbiol* **11**, 128-133

11. Wei, H. L., and Collmer, A. (2012) Multiple lessons from the multiple functions of a regulator of type III secretion system assembly in the plant pathogen Pseudomonas syringae. *Mol Microbiol* **85**, 195-200
12. Martinez-Argudo, I., and Blocker, A. J. (2010) The Shigella T3SS needle transmits a signal for MxiC release, which controls secretion of effectors. *Mol Microbiol* **78**, 1365-1378
13. Lee, P. C., Stopford, C. M., Svenson, A. G., and Rietsch, A. (2010) Control of effector export by the Pseudomonas aeruginosa type III secretion proteins PcrG and PcrV. *Mol Microbiol* **75**, 924-941
14. Cheung, M., Shen, D. K., Makino, F., Kato, T., Roehrich, A. D., Martinez-Argudo, I., Walker, M. L., Murillo, I., Liu, X., Pain, M., Brown, J., Frazer, G., Mantell, J., Mina, P., Todd, T., Sessions, R. B., Namba, K., and Blocker, A. J. (2015) Three-dimensional electron microscopy reconstruction and cysteine-mediated crosslinking provide a model of the type III secretion system needle tip complex. *Mol Microbiol* **95**, 31-50
15. Roehrich, A. D., Guillossou, E., Blocker, A. J., and Martinez-Argudo, I. (2013) Shigella IpaD has a dual role: signal transduction from the type III secretion system needle tip and intracellular secretion regulation. *Mol Microbiol* **87**, 690-706
16. Kenjale, R., Wilson, J., Zenk, S. F., Saurya, S., Picking, W. L., Picking, W. D., and Blocker, A. (2005) The needle component of the type III secreton of Shigella regulates the activity of the secretion apparatus. *J Biol Chem* **280**, 42929-42937
17. Mavris, M., Page, A. L., Tournebize, R., Demers, B., Sansonetti, P., and Parsot, C. (2002) Regulation of transcription by the activity of the Shigella flexneri type III secretion apparatus. *Mol Microbiol* **43**, 1543-1553
18. Pallen, M. J., Beatson, S. A., and Bailey, C. M. (2005) Bioinformatics analysis of the locus for enterocyte effacement provides novel insights into type-III secretion. *BMC Microbiol* **5**, 9
19. Ferracci, F., Schubot, F. D., Waugh, D. S., and Plano, G. V. (2005) Selection and characterization of Yersinia pestis YopN mutants that constitutively block Yop secretion. *Mol Microbiol* **57**, 970-987
20. Schubot, F. D., Jackson, M. W., Penrose, K. J., Cherry, S., Tropea, J. E., Plano, G. V., and Waugh, D. S. (2005) Three-dimensional structure of a macromolecular assembly that regulates type III secretion in Yersinia pestis. *J Mol Biol* **346**, 1147-1161
21. Deane, J. E., Roversi, P., King, C., Johnson, S., and Lea, S. M. (2008) Structures of the *Shigella flexneri* type 3 secretion system protein MxiC reveal conformational variability amongst homologues. *J Mol Biol* **377**, 985-992
22. Buchrieser, C., Glaser, P., Rusniok, C., Nedjari, H., D'Hauteville, H., Kunst, F., Sansonetti, P., and Parsot, C. (2000) The virulence plasmid pWR100 and the repertoire of proteins secreted by the type III secretion apparatus of Shigella flexneri. *Mol Microbiol* **38**, 760-771
23. Botteaux, A., Sory, M. P., Biskri, L., Parsot, C., and Allaoui, A. (2009) MxiC is secreted by and controls the substrate specificity of the Shigella flexneri type III secretion apparatus. *Mol Microbiol* **71**, 449-460
24. Page, A. L., and Parsot, C. (2002) Chaperones of the type III secretion pathway: jacks of all trades. *Mol Microbiol* **46**, 1-11
25. Day, J. B., and Plano, G. V. (1998) A complex composed of SycN and YscB functions as a specific chaperone for YopN in Yersinia pestis. *Mol Microbiol* **30**, 777-788
26. Burkinshaw, B. J., Souza, S. A., and Strynadka, N. C. (2015) Structural analysis of SepL, an enteropathogenic Escherichia coli type III secretion-system gatekeeper protein. *Acta Crystallogr F Struct Biol Commun* **71**, 1300-1308
27. Archuleta, T. L., and Spiller, B. W. (2014) A Gatekeeper Chaperone Complex Directs Translocator Secretion during Type Three Secretion. *PLoS Pathog* **10**, e1004498
28. Wang, D., Roe, A. J., McAteer, S., Shipston, M. J., and Gally, D. L. (2008) Hierarchal type III secretion of translocators and effectors from *Escherichia coli* O157:H7 requires the carboxy terminus of SepL that binds to Tir. *Mol Microbiol* **69**, 1499-1512

29. Joseph, S. S., and Plano, G. V. (2013) The SycN/YscB chaperone-binding domain of YopN is required for the calcium-dependent regulation of Yop secretion by Yersinia pestis. *Frontiers in cellular and infection microbiology* **3**, 1 doi: 10.3389/fcimb.2013.00001
30. Jackson, M. W., Day, J. B., and Plano, G. V. (1998) YscB of Yersinia pestis functions as a specific chaperone for YopN. *J Bacteriol* **180**, 4912-4921
31. Parsot, C., Hamiaux, C., and Page, A. L. (2003) The various and varying roles of specific chaperones in type III secretion systems. *Curr Opin Microbiol* **6**, 7-14
32. Roehrich, A. D. (2013) Regulation of type III secretion hierarchy in Shigella flexneri. *PhD thesis*
33. Cherradi, Y., Schiavolin, L., Moussa, S., Meghraoui, A., Meksem, A., Biskri, L., Azarkan, M., Allaoui, A., and Botteaux, A. (2013) Interplay between predicted inner-rod and gatekeeper in controlling substrate specificity of the type III secretion system. *Mol Microbiol* **87**, 1183-1199
34. Chou, P. Y., and Fasman, G. D. (1978) Empirical predictions of protein conformation. *Annu Rev Biochem* **47**, 251-276
35. Polyhach, Y., Bordignon, E., and Jeschke, G. (2011) Rotamer libraries of spin labelled cysteines for protein studies. *Physical chemistry chemical physics : PCCP* **13**, 2356-2366
36. Kubori, T., and Galan, J. E. (2002) *Salmonella* type III secretion-associated protein InvE controls translocation of effector proteins into host cells. *J Bacteriol* **184**, 4699-4708
37. Silva-Herzog, E., Joseph, S. S., Avery, A. K., Coba, J. A., Wolf, K., Fields, K. A., and Plano, G. V. (2011) Scc1 (CP0432) and Scc4 (CP0033) function as a type III secretion chaperone for CopN of Chlamydia pneumoniae. *J Bacteriol* **193**, 3490-3496
38. Archuleta, T. L., Du, Y., English, C. A., Lory, S., Lesser, C., Ohi, M. D., Ohi, R., and Spiller, B. W. (2011) The Chlamydia effector chlamydial outer protein N (CopN) sequesters tubulin and prevents microtubule assembly. *J Biol Chem* **286**, 33992-33998
39. Birket, S. E., Harrington, A. T., Espina, M., Smith, N. D., Terry, C. M., Darboe, N., Markham, A. P., Middaugh, C. R., Picking, W. L., and Picking, W. D. (2007) Preparation and characterization of translocator/chaperone complexes and their component proteins from Shigella flexneri. *Biochemistry* **46**, 8128-8137
40. Lee, P. C., Zmina, S. E., Stopford, C. M., Toska, J., and Rietsch, A. (2014) Control of type III secretion activity and substrate specificity by the cytoplasmic regulator PcrG. *Proc Natl Acad Sci U S A* **111**, E2027-2036
41. Shen, D. K., and Blocker, A. J. (2016) MxiA, MxiC and IpaD Regulate Substrate Selection and Secretion Mode in the T3SS of Shigella flexneri. *PLoS One* **11**, e0155141
42. Johnson, S., Roversi, P., Espina, M., Olive, A., Deane, J. E., Birket, S., Field, T., Picking, W. D., Blocker, A. J., Galyov, E. E., Picking, W. L., and Lea, S. M. (2007) Self-chaperoning of the type III secretion system needle tip proteins IpaD and BipD. *J Biol Chem* **282**, 4035-4044
43. Yu, X. J., McGourty, K., Liu, M., Unsworth, K. E., and Holden, D. W. (2010) pH sensing by intracellular Salmonella induces effector translocation. *Science* **328**, 1040-1043
44. Page, A. L., Fromont-Racine, M., Sansonetti, P., Legrain, P., and Parsot, C. (2001) Characterization of the interaction partners of secreted proteins and chaperones of Shigella flexneri. *Mol Microbiol* **42**, 1133-1145
45. Wang, R. F., and Kushner, S. R. (1991) Construction of versatile low-copy-number vectors for cloning, sequencing and gene expression in Escherichia coli. *Gene* **100**, 195-199
46. Datsenko, K. A., and Wanner, B. L. (2000) One-step inactivation of chromosomal genes in Escherichia coli K-12 using PCR products. *Proc Natl Acad Sci U S A* **97**, 6640-6645
47. Bahrani, F. K., Sansonetti, P. J., and Parsot, C. (1997) Secretion of Ipa proteins by Shigella flexneri: inducer molecules and kinetics of activation. *Infect Immun* **65**, 4005-4010
48. Parsot, C., Menard, R., Gounon, P., and Sansonetti, P. J. (1995) Enhanced secretion through the Shigella flexneri Mxi-Spa translocon leads to assembly of extracellular proteins into macromolecular structures. *Mol Microbiol* **16**, 291-300
49. Barzu, S., Nato, F., Rouyre, S., Mazie, J. C., Sansonetti, P., and Phalipon, A. (1993) Characterization of B-cell epitopes on IpaB, an invasion-associated antigen of Shigella flexneri:

identification of an immunodominant domain recognized during natural infection. *Infect Immun* **61**, 3825-3831
50. Phalipon, A., Arondel, J., Nato, F., Rouyre, S., Mazie, J. C., and Sansonetti, P. J. (1992) Identification and characterization of B-cell epitopes of IpaC, an invasion-associated protein of Shigella flexneri. *Infect Immun* **60**, 1919-1926
51. Menard, R., Sansonetti, P. J., and Parsot, C. (1993) Nonpolar mutagenesis of the ipa genes defines IpaB, IpaC, and IpaD as effectors of Shigella flexneri entry into epithelial cells. *J Bacteriol* **175**, 5899-5906
52. Jeschke, G. (2012) DEER distance measurements on proteins. *Annu Rev Phys Chem* **63**, 419-446
53. Lillington, J. E., Lovett, J. E., Johnson, S., Roversi, P., Timmel, C. R., and Lea, S. M. (2011) Shigella flexneri Spa15 crystal structure verified in solution by double electron electron resonance. *J Mol Biol* **405**, 427-435
54. Johnson, S., Roversi, P., Espina, M., Deane, J. E., Birket, S., Picking, W. D., Blocker, A., Picking, W. L., and Lea, S. M. (2006) Expression, limited proteolysis and preliminary crystallographic analysis of IpaD, a component of the Shigella flexneri type III secretion system. *Acta Crystallograph Sect F Struct Biol Cryst Commun* **62**, 865-868
55. Jeschke, G., Chechik, V., Ionita, P., Godt, A., Zimmermann, H., Banham, J., Timmel, C. R., Hilger, D., and Jung, H. (2006) DeerAnalysis2006—a comprehensive software package for analyzing pulsed ELDOR data. *Appl Magn Reson* **30**, 473–498

FOOTNOTES

[a]Current address: Testo AG, Testostraße 1, 79853 Lenzkirch, Germany
[b]Current address: Ruhr-Universität Bochum, Faculty of Chemistry and Biochemistry, Universitätsstraße 150, 44780 Bochum, Germany

TABLE 1. Phenotypic overview of mutants

Mutant	Design group	MxiC			Translocators		Effectors	in *mxiHK69A* background		Phenotypic class	Main secretion defect
		leaked	induced	in Δ*ipaB*	leaked	induced	overall	MxiC leaked	IpgD/IpaA leaked		
Wild-type	NA	–	+++	+++	–	+++++	–	–	NA	NA	NA
Δ*mxiC*	NA	NA	NA	NA	–	+	+++	NA	+	0	Null (Translocators/ Effectors)
Δ*mxiC/mxiC*	NA	–	+++	+++	–	++++	–	–	–	NA	NA
*mxiC*Δ*Cterm*	Cterm	ND	+	+	–	+	+++	–/+	+	0	Near null
*mxiC*Δ*Nterm*	Nterm	–	–	–	–	+++	+++	ND	ND	1a	MxiC/Effectors
*mxiC*Δ*CBD*	CBD	+	–	+++	–	++++	+++	–/+	+	1a	MxiC/Effectors
mxiCK66E	CBD	++	++[a]	ND	–	++	+++	–	+	1b	MxiC leaked/Effector
mxiCK68E	CBD	+++	+++	ND	–	++	+++	–	–	1c	MxiC leaked
mxiC(M226K,L242D; hydrophobic)	hydro.	–/+	+++	ND	–	+++	+++	–/+	+	1d	Effector
mxiC(E201K,E276K, E293; negative)	neg.	++	+++	ND	+++[b]	++++[c]	++	–/+	+	2	Translocators
mxiC (I251A,T253A,S254A, D255E; straight)	hinge	–	+++	ND	–	++++[d]	–	ND	ND	2	Translocators
mxiCV256P	hinge	–	+	+	–	+++	+++[e]	–	+	1a	MxiC/Effectors
mxiC(T253G,S254G, D255G; wobble)	hinge	–	+	ND	–	++	+++	ND	ND	1a	MxiC/Effectors

[a]poorly detected in whole cell lysate; [b] IpaB/C increased; [c] not IpaD; [d] IpaC/B reduced, IpaD slightly increased; [e] IpgB1 increased

FIGURE LEGENDS

FIGURE 1. Location of MxiC mutations used in this work. *Top*, MxiC structure 2VJ4 (chain A) coloured from blue at the N-terminus, where MxiC74 is the first residue in the first crystallised helix, to red at the C-terminus. Therefore N-terminus and most of CBD are not shown. *Below*, same MxiC rotated by 90° about its long axis. Mutated residues are coloured according to their design group, as labeled on the figure. In orange are mutations in the hydrophobic core of the protein, made by others (19,33)**,** which lead to loss of function.

FIGURE 2. MxiC without its secretion signal is still able to promote inducible translocator secretion**.** (A) Protein secretion in response to the artificial inducer Congo red (CR). Samples from *Shigella* wild-type, *ΔmxiC* mutant, complemented strain (*ΔmxiC*/*mxiC*+, grown with 25 µM IPTG) and *mxiCΔNterm* (in the *ΔmxiC* background, grown with 100 µM IPTG) were collected as described in the Experimental Procedures, Silver stained (top panel) and Western-blotted with the indicated antibodies (bottom panels). All samples probed with the same antibody were analysed on the same gel. Results shown are representative of at least two independent experiments. (B) Total protein expression levels in whole culture lysates. Samples were collected as described in the Experimental Procedures and Western-blotted with the indicated antibodies. (C) Quantification of translocator secretion after CR induction. Samples from two independent experiments, one of them performed in duplicate, were quantified on Western blots. The averages and standard deviations of the wild-type-normalised data are displayed. There is an overall difference between proteins and strains in an ANOVA ($p < 0.01$ and $p < 0.001$, respectively). In pairwise comparisons, the difference between *ΔmxiC* and both the complemented strain and *mxiCΔNterm* is statistically significant (post hoc test with Bonferroni correction, $p < 0.001$ and $p < 0.01$, respectively), while the difference between complemented strain and *mxiCΔNterm* is not significant.

FIGURE 3. The putative chaperone-binding domain regulates MxiC secretion and is required for blocking effector secretion. (A) Protein secretion in response to the artificial inducer Congo red (CR). Samples from the complemented strain (*ΔmxiC*/*mxiC*+) and indicated *mxiC* mutants (in the *ΔmxiC* background) were collected as described in the Experimental Procedures, Silver-stained (top panel) and Western-blotted with the indicated antibodies (bottom panels). (B) Exponential leakage. Samples were collected as described in the Experimental Procedures, Silver-stained (top panel) and Western-blotted with the indicated antibodies (bottom panels). (C) Total protein expression levels in whole culture lysates. Samples were collected as described in the Experimental Procedures and Western-blotted with the indicated antibodies. Results shown are representative of at least two independent experiments.

FIGURE 4. The conserved hydrophobic patch on the surface of MxiC is involved in preventing effector secretion. (A) Protein secretion in response to the artificial inducer Congo red (CR). *Shigella* wildtype, *ΔmxiC* mutant, complemented strain (*ΔmxiC*/*mxiC*+) and *mxiC(M226K,L242D)* (in the *ΔmxiC* background) were grown with 25 µM IPTG where required. Samples were collected as described in the Experimental Procedures, Silver-stained (*top panel*) and Western-blotted with the indicated antibodies (*bottom panels*). (B) Exponential leakage. Samples were collected as described in the Experimental Procedures, Silver-stained (*top panel*) and Western-blotted with the indicated antibodies (*bottom panels*). (C) Total protein expression levels in whole culture lysates. Samples were collected as described in the Experimental Procedures and Western-blotted with the indicated antibodies. Results shown are representative of at least two independent experiments.

FIGURE 5. Mutants designed to alter the conformation of MxiC show opposed phenotypes. (A) Protein secretion in response to the artificial inducer Congo red (CR). *Shigella* wild-type, *ΔmxiC* mutant, complemented strain (*ΔmxiC*/*mxiC*+) and *mxiC* mutants (in the *ΔmxiC* background) were grown with 25 µM IPTG where required. Mutant *mxiC(T253G,S254G,D255G)* is abbreviated *mxiC(wobble)* and mutant

mxiC(I251A,T253A,S254A,D255E) is abbreviated *mxiC(straight)*. Samples were collected as described in the Experimental Procedures, Silver-stained (*top panel*) and Western-blotted with the indicated antibodies (*bottom panels*). (B) Exponential leakage. Samples were collected as described in the Experimental Procedures, Silver-stained (*top panel*) and Western-blotted with the indicated antibodies (*bottom panels*). (C) Total protein expression levels in whole culture lysates. Samples were collected as described in the Experimental Procedures and Western-blotted with the indicated antibodies. (D) Quantification of translocator secretion after CR induction. Samples from three independent experiments were quantified on Western blots and normalised against the complemented strain *ΔmxiC*/*mxiC*+. The averages and standard deviations are displayed. There is an overall difference between proteins and strains in an ANOVA ($p < 0.01$ and $p < 0.001$, respectively). In pairwise comparisons (post hoc test with Bonferroni correction), the difference between *mxiC(T253G,S254G,D255G)* and *ΔmxiC*/*mxiC*+ is statistically significant ($p < 0.001$), the same is true for mutant *mxiCV256P*. Both strains are not significantly different from the *ΔmxiC* mutant. Mutant *mxiC(I251A, T253A,S254A,D255E)* is overall significantly different from *ΔmxiC* ($p < 0.001$), but not from the complemented strain. There are also significant differences between proteins in the *mxiC(I251A,T253A,S254A,D255E)* mutant ($p < 0.01$ in an ANOVA). Specifically, IpaD is significantly different from both IpaB and IpaC (post hoc test with Bonferroni correction, $p < 0.05$ and $p < 0.01$, respectively).

FIGURE 6. His-MxiC(Cys) is nearly completely labelled with MTSL and the 247-290 interspin distance distribution is between that of the "straight" and "bent" forms. His-MxiC(Cys) was modified with MTSL as described in Experimental Procedures. The labelling efficiency was assessed using room temperature continuous wave EPR. The resulting EPR derivative signal is displayed in arbitrary units (a.u.). (A) Labelling efficiency in His-MxiC(Cys) alone. The spin concentration is ca. 66 μM and ~100% of His-MxiC(Cys) was modified by MTSL (the residual free label fraction is marked with an asterisk). (B) and (C) In the left column, V(t)/V(0) is the primary DEER data, the inset in B shows the background-corrected F(t)/F(0) with the fit (red dotted line). In the right column, P(r) is the probability for the different distances extracted with model-free Tikhonov regularization using DeerAnalysis. The red dotted lines show the simulation by MMM. (B) Comparison of the "bent" MxiC model with the experimental data for His-MxiC(Cys). (C) Comparison of the MxiC crystal structure (PDB code 2VJ4, chain A) with the experimental data for His-MxiC(Cys). Comparisons with all other chains in all crystal structures are shown in supplemental Fig. S11. The chain presented in this panel was chosen because it was used as template to model the "bent" form of MxiC.

FIGURE 7. Continuous wave EPR detects a weak but specific interaction of MxiC with IpaD. (A) Continuous wave (cw) EPR spectrum of spin-labeled MxiC in the absence (*black*) and in the presence of 10-fold excess of Spa15 (*cyan*). (B) cw EPR spectrum of spin-labelled MxiC in the absence (*black*) and in the presence of 10-fold excess of IpgC (*red*) or IpgC-IpaC (*orange*). (C) *Left*, cw EPR spectrum of spin-labelled MxiC in the absence (*black*) and in the presence of 10-fold excess of IpaD (*green*) or IpaD-IpagC-IpaC (*red*). *Right*, the magnified low field region of the spectra (331.5-334.5 mT) highlights the detectable spectral differences. (D) Cw EPR spectrum of spin-labelled MxiC in the absence (*black*) in the absence (*black*) and in the presence of n-fold excess of IpaD (*indicated in the legend*). (E) Cw EPR spectrum of spin-labelled MxiC in the absence (*black*) and in the presence of 10-fold excess of IpaD (*green*), and after 1:4 dilution (*olive green*). The inset shows the magnified low field region of the spectra (331.5-334.5 mT) which highlights the fact that upon dilution, the spectrum reverts to that of MxiC alone (except for a small fraction of free label, see *asterisks*), indicating that complex formation can be detected only at high protein concentrations due to the low affinity. The normalisation of the spectral intensity of the diluted sample was done where indicated by the arrow to remove the effect of the free label. Except where otherwise stated, the spectra are normalised to the maximum amplitude of the central EPR line. The insets show the magnified low field region of the spectra (331.5-334.5 mT) to highlight possible spectral differences. The stars highlight the minor fraction of label, which is released during the incubation with some protein complexes and/or upon dilution.

FIGURE 8. Analysis of *mxiC* mutant phenotypes in the mxiHK69A background. Protein secretion in response to the artificial inducer Congo red (CR). *Shigella* wild-type, *ΔmxiCΔmxiH* mutant, complemented strains (*ΔmxiCΔmxiH*/*mxiCmxiH* or *ΔmxiCΔmxiH*/*mxiCmxiHK69A*) and *mxiC* mutants (in the *ΔmxiCΔmxiH* background expressing either *mxiH or mxiHK69A*) were grown with 25 μM IPTG where required. Mutants *mxiC(E201K,E276K,E293)* and *mxiC(M226K,L242D)* are abbreviated *mxiC(negative)* and *mxiC(hydrophobic)*, respectively. Samples were collected as described in the Experimental Procedures, Silver-stained (*top panel*) and Western-blotted with the indicated antibodies (*bottom panels*). Arrow indicates faster migration of *MxiCΔCBD.*

FIGURE 9. Modelling of MxiC-IpaD interaction. (A) Docking of gray MxiC (PDB entry 2VJ4 chain A (residues 64 – 349), (21), pink) and coloured IpaD (PDB entry 2J0O chain A, (42)). The N-terminal domain of IpaD is coloured in blue (residues 40-130), the C-terminal globular domain is coloured in red (residues 177-271) and the coiled coil domain is coloured in green (residues 131-176 and 272-321). Residues Glu201, Glu276 and Glu293 involved in the negatively charged patch of MxiC are highlight as space-fill model. The *bottom* panel is rotated 90 ° around the x-axis compared with the top panel illustrating the elongated shape of the dimer. (B) The interface of the MxiC IpaD dimer shows complementary charges. The *top* panel shows the electrostatic potential surface of IpaD and the backbone of MxiC, the *bottom* panel shows the electrostatic potential surface of MxiC and the backbone of IpaD. The panels are rotated 180° with respect to each other. Negative charges are shown in red, positive charges are depicted in blue. The docking was performed manually using the location of *ipaD* and *mxiC* mutants. The model was generated in Insight II 2005 and optimized using Discover 2.98. Electrostatic potential surfaces were calculated using Delphi (all Accelrys Inc.).

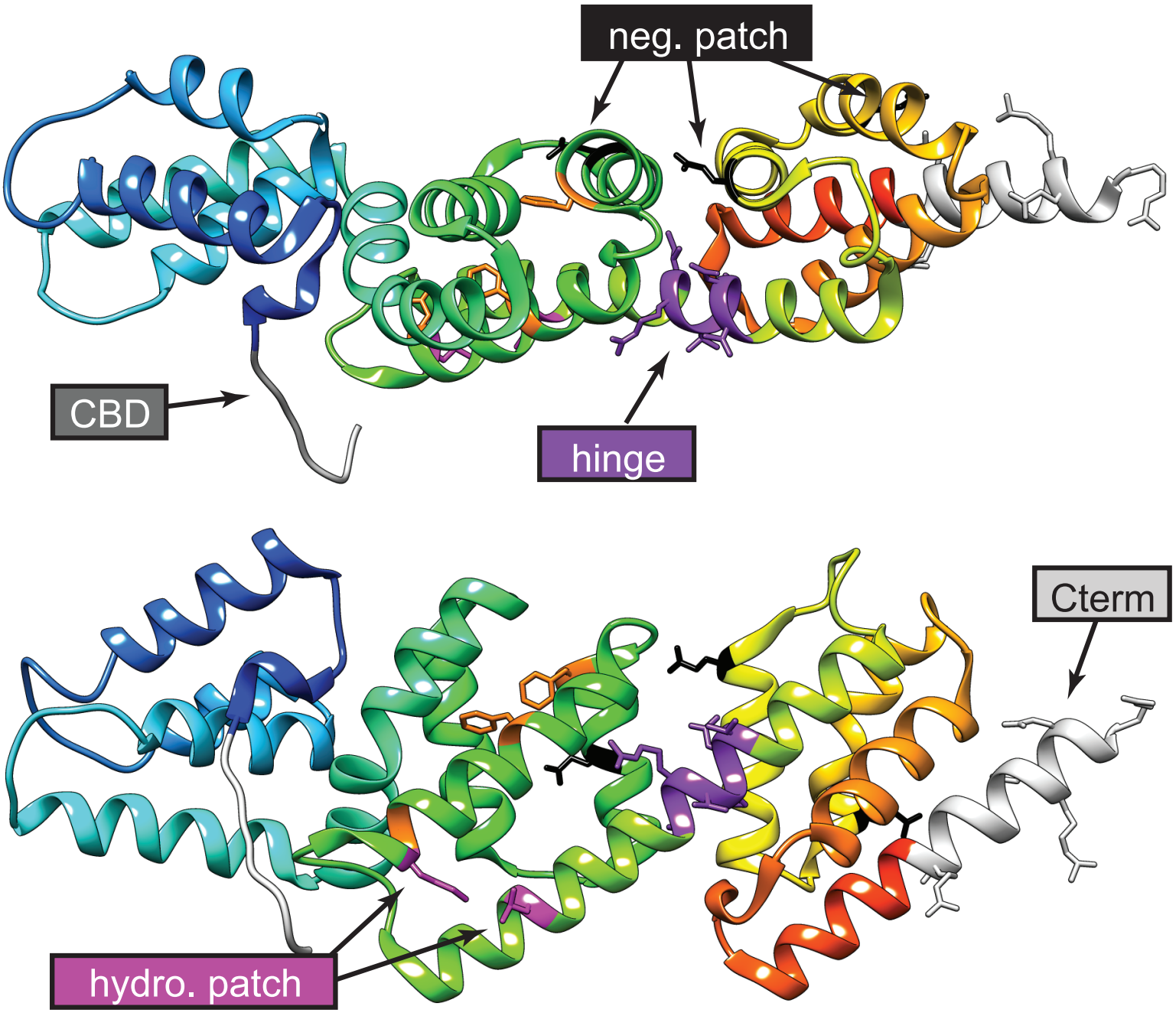
neg. patch
CBD
hinge
Cterm
hydro. patch

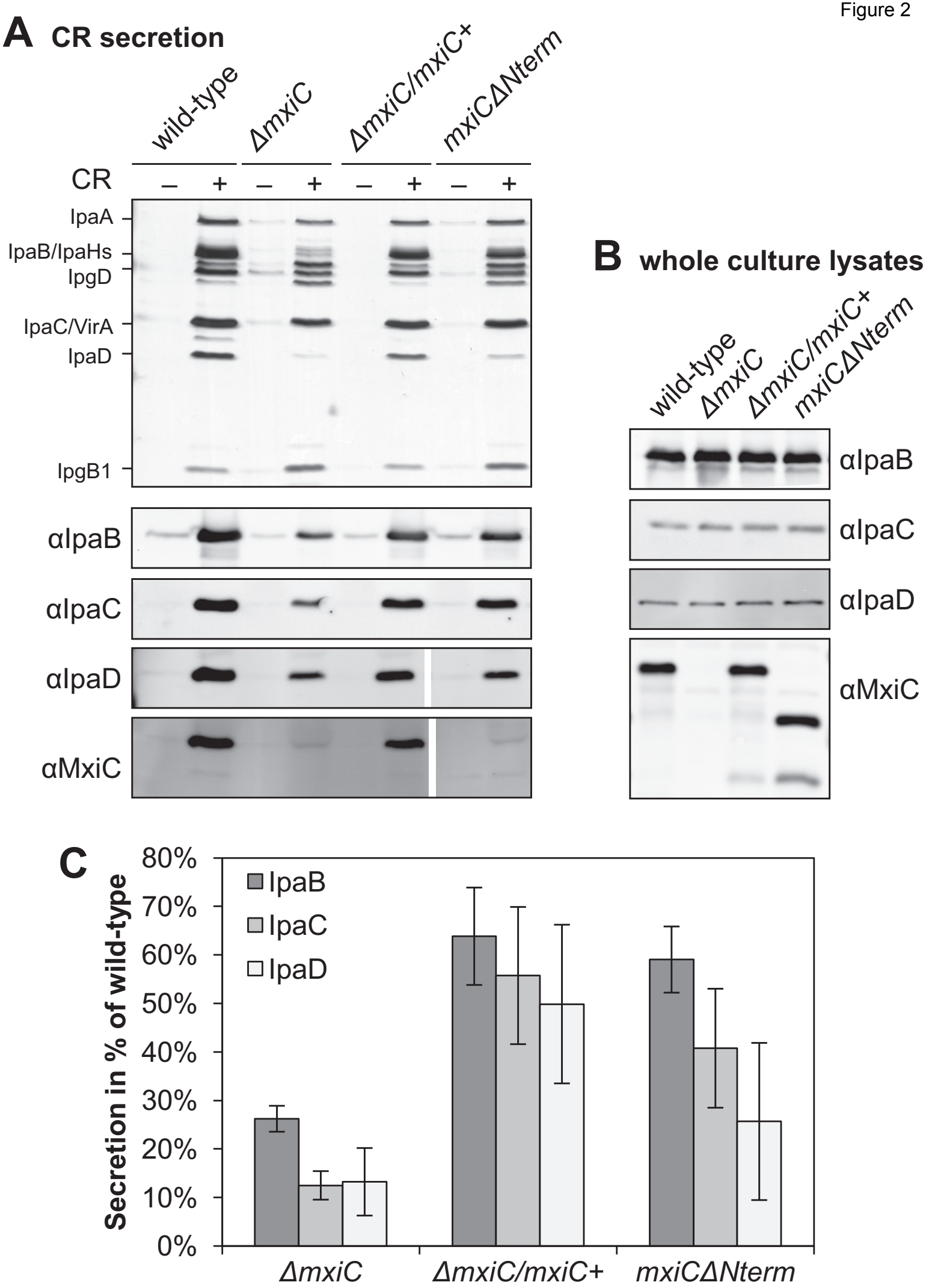
A CR secretion
wild-type
ΔmxiC
ΔmxiC/mxiC+
mxiCΔNterm
CR
– + – + – + – +
IpaA
IpaB/IpaHs
IpgD
IpaC/VirA
IpaD
IpgB1
αIpaB
αIpaC
αIpaD
αMxiC
B whole culture lysates
wild-type
ΔmxiC
ΔmxiC/mxiC+
mxiCΔNterm
αIpaB
αIpaC
αIpaD
αMxiC
C
Secretion in % of wild-type
80%
70%
60%
50%
40%
30%
20%
10%
0%
IpaB
IpaC
IpaD
ΔmxiC
ΔmxiC/mxiC+
mxiCΔNterm

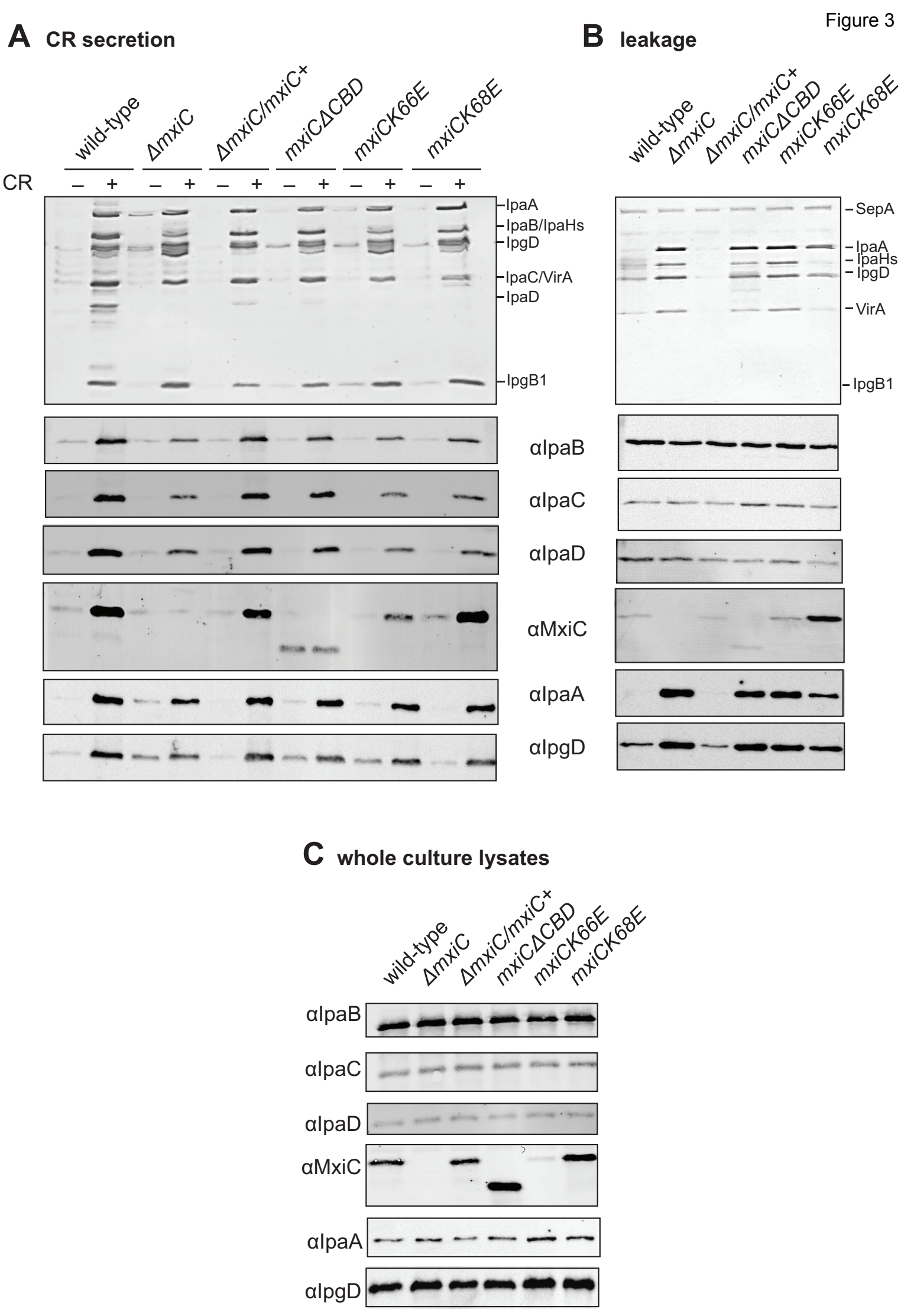
A CR secretion
B leakage
wild-type
ΔmxiC
ΔmxiC/mxiC+
mxiCΔCBD
mxiCK66E
mxiCK68E
CR
– + – + – + – + – + – +
IpaA
IpaB/IpaHs
IpgD
IpaC/VirA
IpaD
IpgB1
SepA
IpaA
IpaHs
IpgD
VirA
IpgB1
αIpaB
αIpaC
αIpaD
αMxiC
αIpaA
αIpgD
C whole culture lysates
wild-type
ΔmxiC
ΔmxiC/mxiC+
mxiCΔCBD
mxiCK66E
mxiCK68E
αIpaB
αIpaC
αIpaD
αMxiC
αIpaA
αIpgD

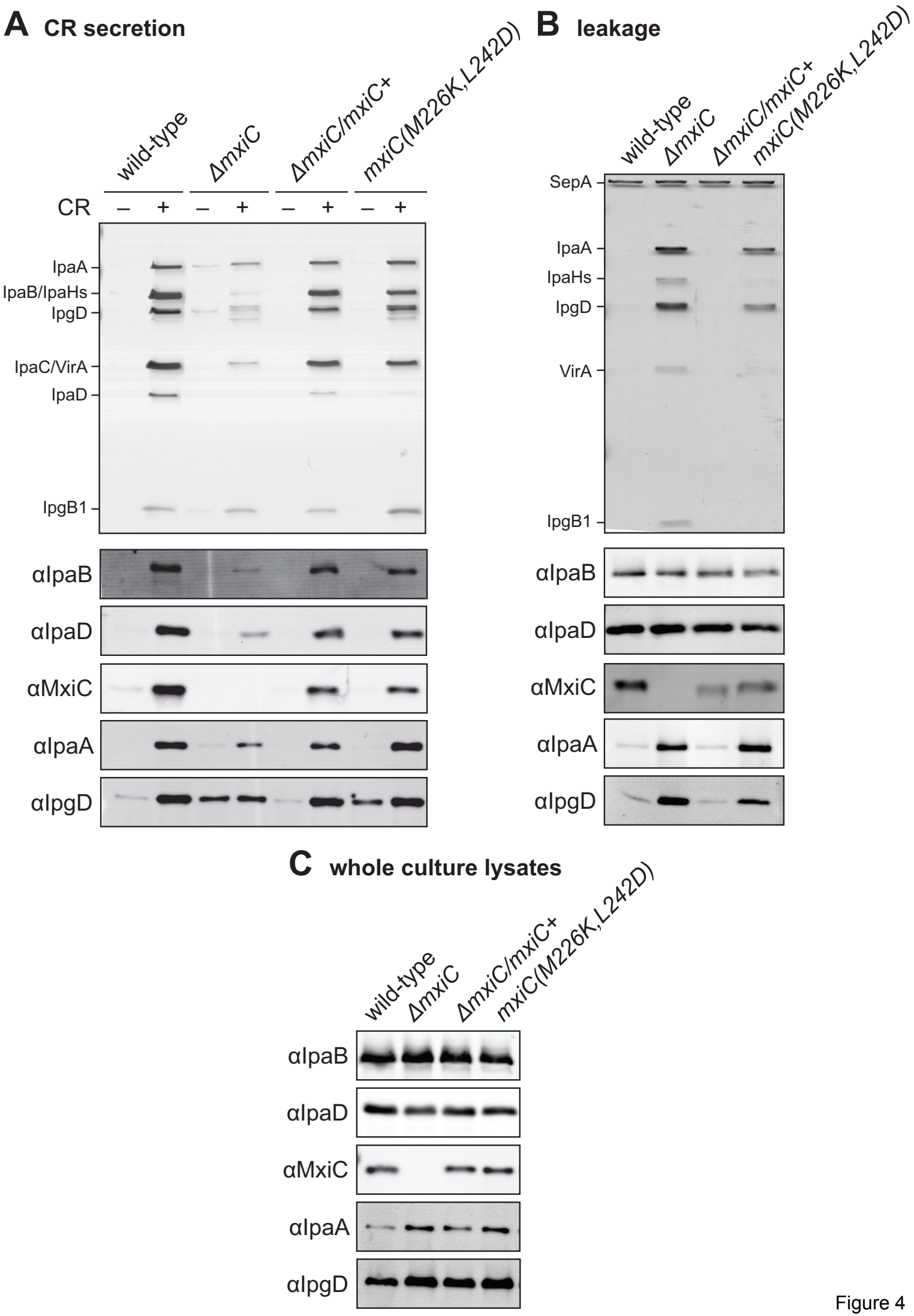
A CR secretion
wild-type
ΔmxiC
ΔmxiC/mxiC+
mxiC(M226K,L242D)
CR
– + – + – + – +
IpaA
IpaB/IpaHs
IpgD
IpaC/VirA
IpaD
IpgB1
αIpaB
αIpaD
αMxiC
αIpaA
αIpgD
B leakage
wild-type
ΔmxiC
ΔmxiC/mxiC+
mxiC(M226K,L242D)
SepA
IpaA
IpaHs
IpgD
VirA
IpgB1
αIpaB
αIpaD
αMxiC
αIpaA
αIpgD
C whole culture lysates
wild-type
ΔmxiC
ΔmxiC/mxiC+
mxiC(M226K,L242D)
αIpaB
αIpaD
αMxiC
αIpaA
αIpgD

Figure 4

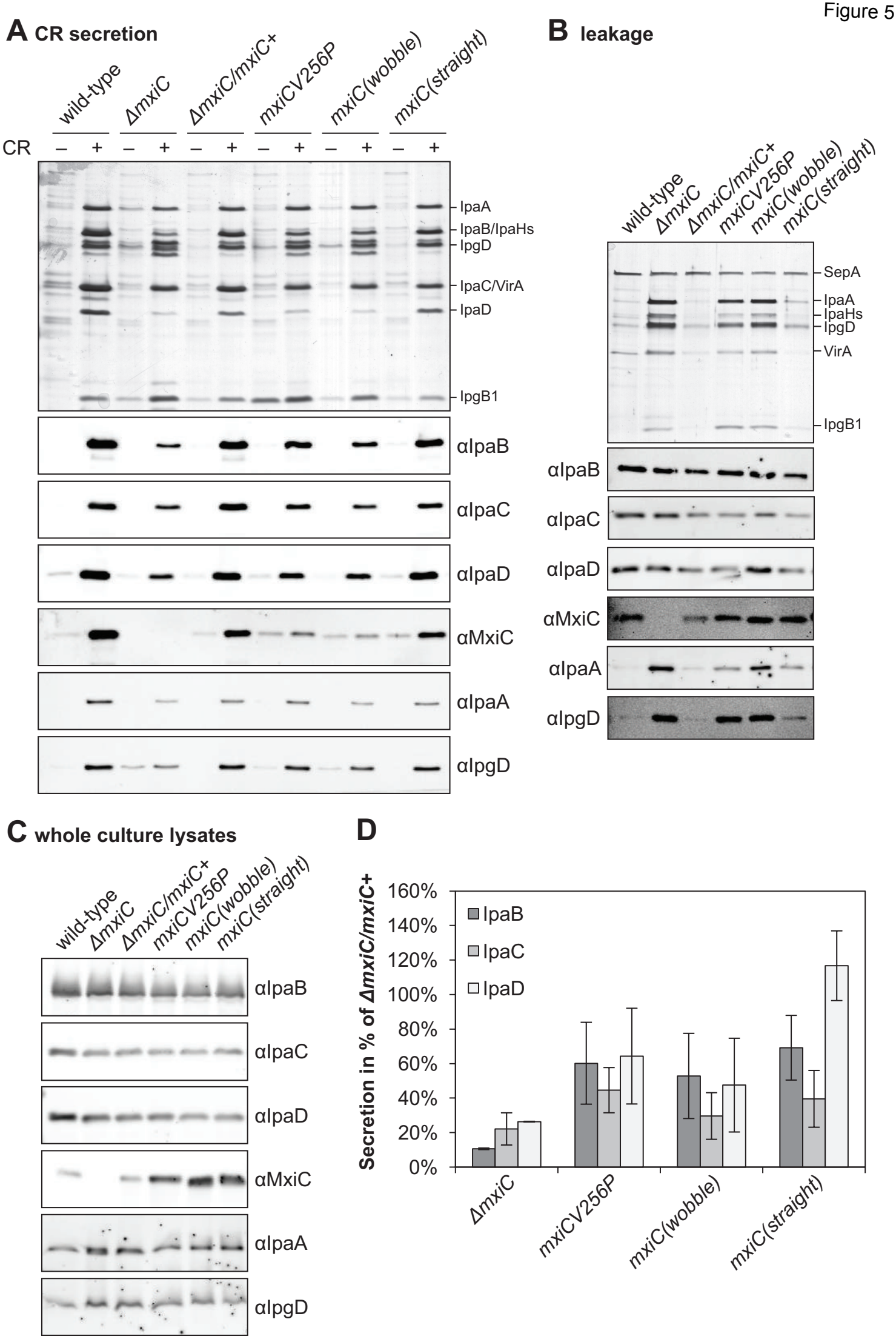
A CR secretion
wild-type
ΔmxiC
ΔmxiC/mxiC+
mxiCV256P
mxiC(wobble)
mxiC(straight)
CR
– + – + – + – + – + – +
IpaA
IpaB/IpaHs
IpgD
IpaC/VirA
IpaD
IpgB1
αIpaB
αIpaC
αIpaD
αMxiC
αIpaA
αIpgD
B leakage
wild-type
ΔmxiC
ΔmxiC/mxiC+
mxiCV256P
mxiC(wobble)
mxiC(straight)
SepA
IpaA
IpaHs
IpgD
VirA
IpgB1
αIpaB
αIpaC
αIpaD
αMxiC
αIpaA
αIpgD
C whole culture lysates
wild-type
ΔmxiC
ΔmxiC/mxiC+
mxiCV256P
mxiC(wobble)
mxiC(straight)
αIpaB
αIpaC
αIpaD
αMxiC
αIpaA
αIpgD
D
Secretion in % of ΔmxiC/mxiC+
160%
140%
120%
100%
80%
60%
40%
20%
0%
IpaB
IpaC
IpaD
ΔmxiC
mxiCV256P
mxiC(wobble)
mxiC(straight)

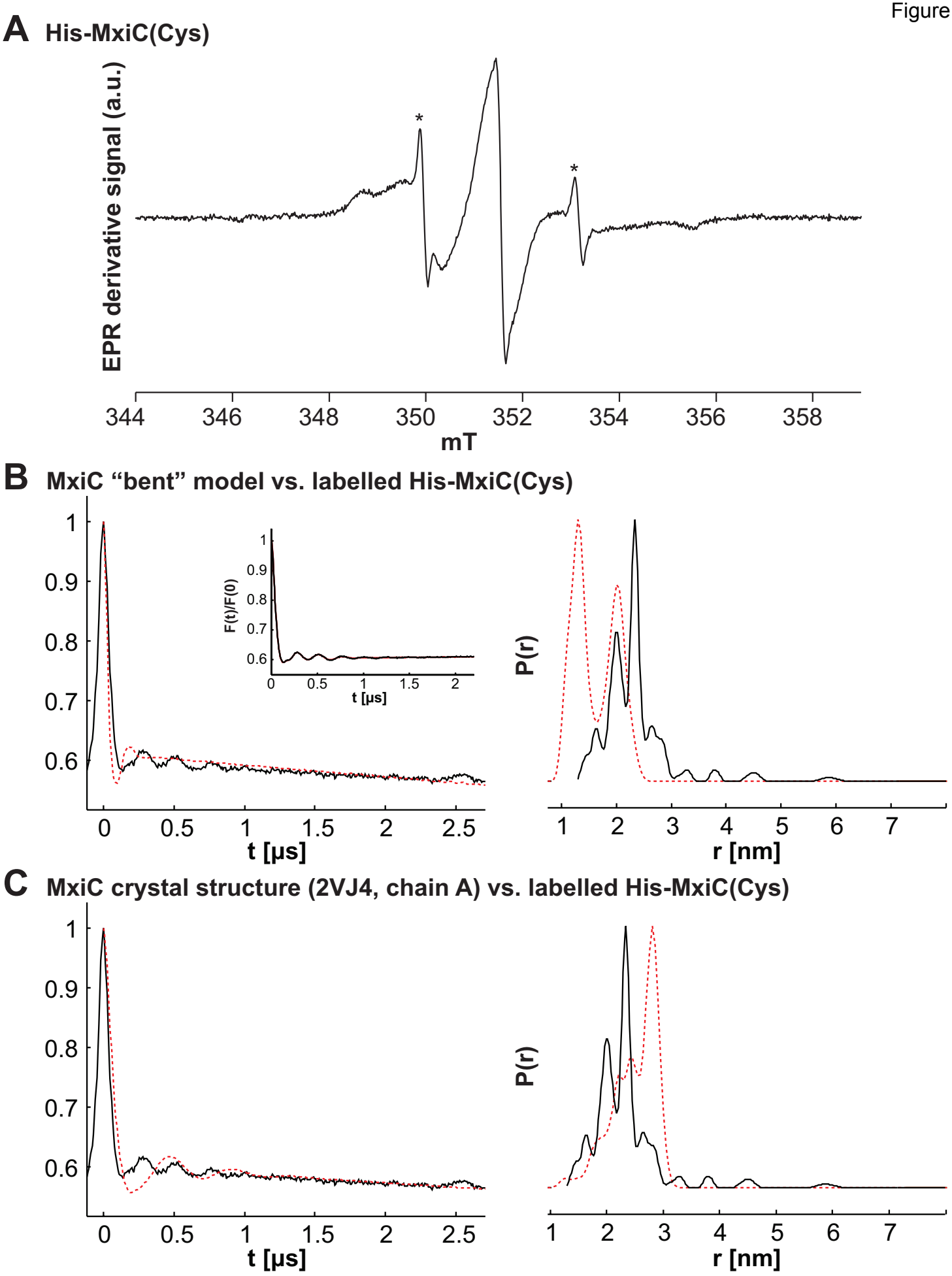
A
His-MxiC(Cys)
EPR derivative signal (a.u.)
*
*
344
346
348
350
352
354
356
358
mT
B
MxiC "bent" model vs. labelled His-MxiC(Cys)
F(t)/F(0)
t [µs]
P(r)
r [nm]
C
MxiC crystal structure (2VJ4, chain A) vs. labelled His-MxiC(Cys)
P(r)
r [nm]

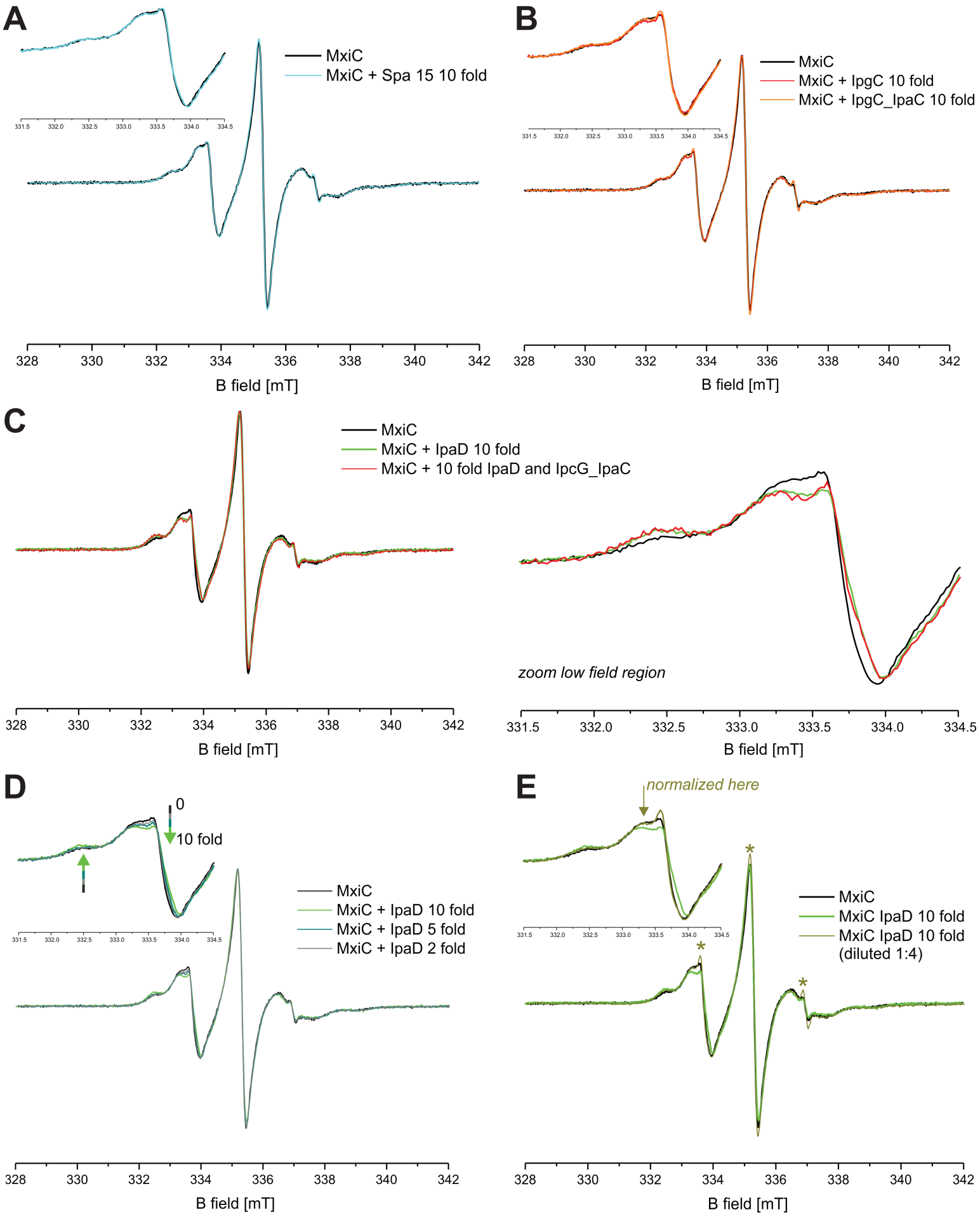
A
MxiC
MxiC + Spa 15 10 fold
B field [mT]
B
MxiC
MxiC + IpgC 10 fold
MxiC + IpgC_IpaC 10 fold
B field [mT]
C
MxiC
MxiC + IpaD 10 fold
MxiC + 10 fold IpaD and IpcG_IpaC
zoom low field region
B field [mT]
B field [mT]
D
0
10 fold
MxiC
MxiC + IpaD 10 fold
MxiC + IpaD 5 fold
MxiC + IpaD 2 fold
B field [mT]
E
normalized here
MxiC
MxiC IpaD 10 fold
MxiC IpaD 10 fold
(diluted 1:4)
B field [mT]

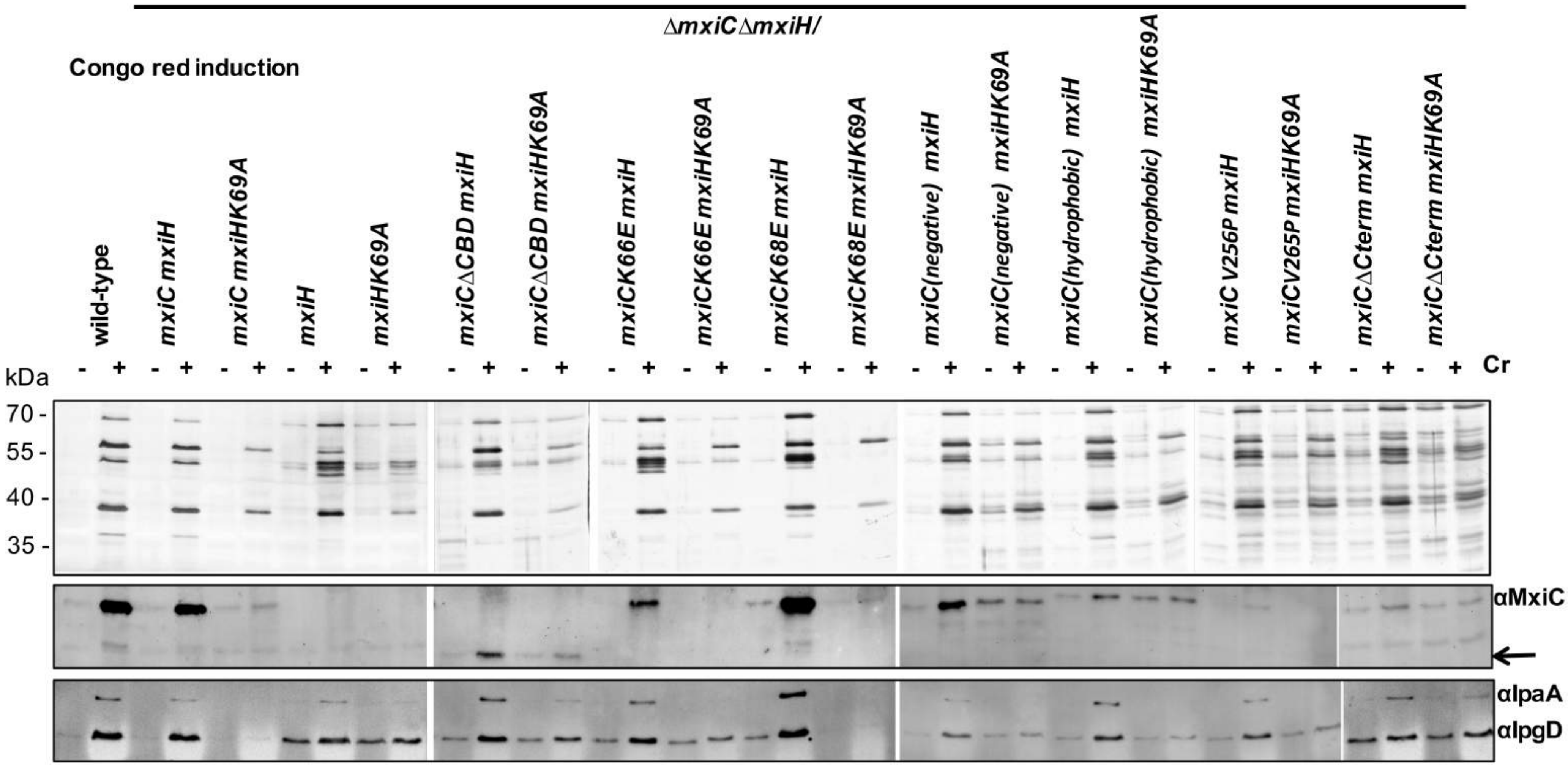
Congo red induction
ΔmxiCΔmxiH/
wild-type
mxiC mxiH
mxiC mxiHK69A
mxiH
mxiHK69A
mxiCΔCBD mxiH
mxiCΔCBD mxiHK69A
mxiCK66E mxiH
mxiCK66E mxiHK69A
mxiCK68E mxiH
mxiCK68E mxiHK69A
mxiC(negative) mxiH
mxiC(negative) mxiHK69A
mxiC(hydrophobic) mxiH
mxiC(hydrophobic) mxiHK69A
mxiC V256P mxiH
mxiCV265P mxiHK69A
mxiCΔCterm mxiH
mxiCΔCterm mxiHK69A
Cr
kDa
70
55
40
35
αMxiC
αIpaA
αIpgD

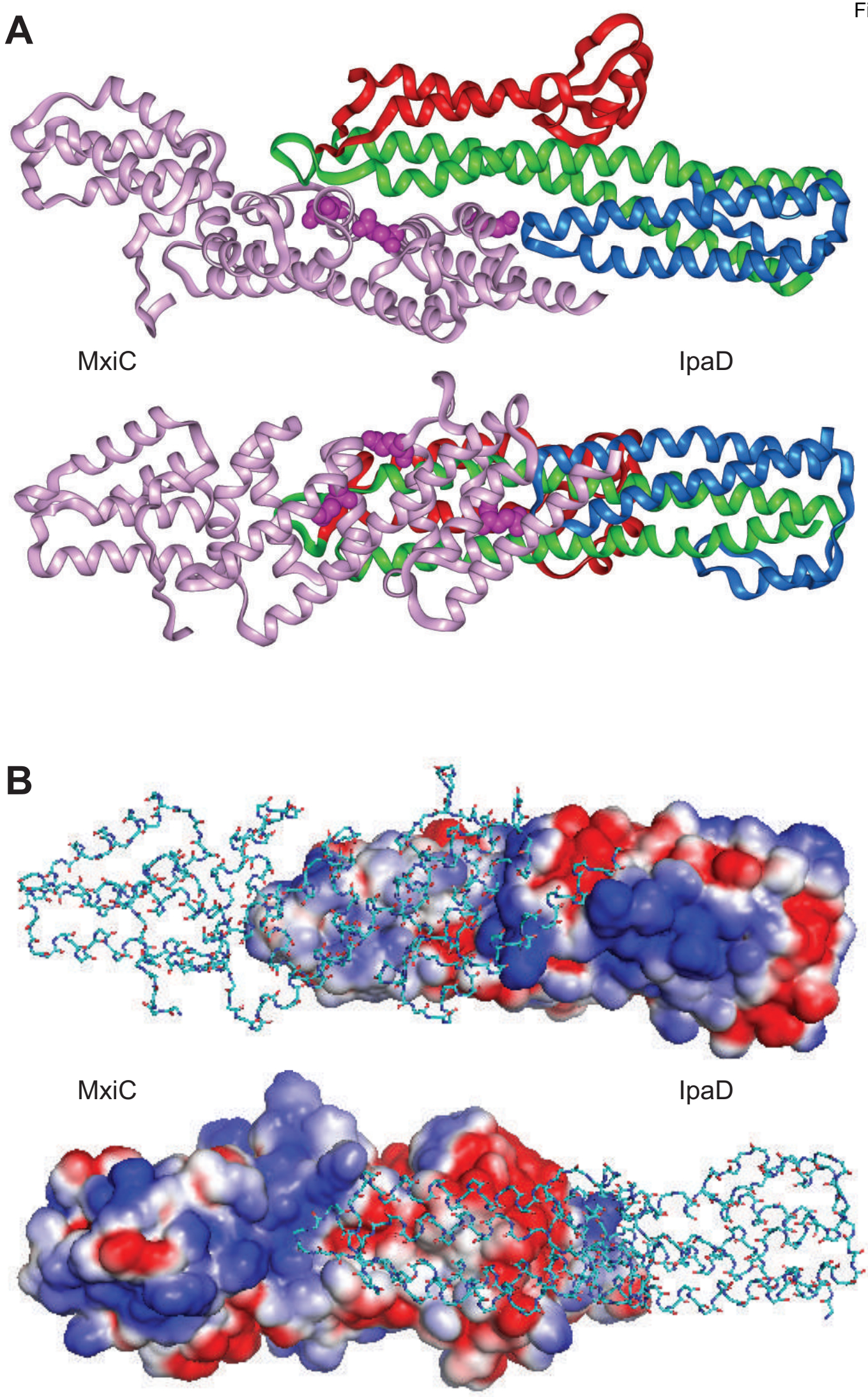
A
MxiC
IpaD
B
MxiC
IpaD